Chapter 1
Nanotechnology for Water and Wastewater Treatment Using Graphene Semiconductor Composite Materials

Francis Opoku, Ephraim M. Kiarii, and Penny P. Govender

Contents

Abstract Recently, contamination of water resources has become a persistent problem to human due to advanced industrialization and rapid population growth. The major causes of water pollution are dye effluents from textile dyeing, pharmaceuticals, and paper printing industries. Therefore, cost-effective technologies, such as membrane filtration, adsorption, coagulation, microbial degradation, and chemical oxidation, are adopted for the removal of pollutants from water effluents. Graphene-based materials have gained much consideration as a novel material for

F. Opoku · E. M. Kiarii · P. P. Govender (✉)
Department of Applied Chemistry, University of Johannesburg, Johannesburg, South Africa
e-mail: pennyg@uj.ac.za

N. Dasgupta et al. (eds.), *Environmental Nanotechnology Volume 4*, Environmental Chemistry for a Sustainable World 32, https://doi.org/10.1007/978-3-030-26668-4_1

addressing the global environmental issues due their high mechanical strength, excellent electron mobility, large surface area, and high thermal conductivity. Semiconductor photocatalysis has received much interest as a promising technology for water treatment owing to its cost-effective, easy operation, high-efficiency, and convenience. Therefore, the design and fabrication of graphene support with semiconductor photocatalyst are promising as multifunctional catalysts. This book chapter evaluates the recent design of graphene-based materials as adsorbent and photocatalytic materials in environmental remediation. The theoretical outcomes in water treatment using graphene/semiconductor composites are also summarized. A brief outlook on the challenges and new strategies is provided for developing effective water/wastewater treatment techniques using graphene-based materials.

Keywords Nanotechnology · Water treatments · Photocatalyst · Semiconductor · Composites

1.1 Introduction

The release of municipal, agricultural, industrial, and domestic waste effluents into water resources has certainly given rise to a lot of toxic contaminants (Marahel et al. 2015). Heavy metal ions and dyes have attracted serious concern owing to their non-biodegradable, high toxicity and tend to accumulate in the tissues of living organisms (Fu and Wang 2011a). The highly toxic and non-biodegradable of most dye molecules is due to the aromatic ring in their structure (Hou et al. 2012). Furthermore, dyes add adverse color to water resources, which prevent the penetration of sunlight to retard photosynthetic reactions, thereby affecting aquatic life (Marahel et al. 2015). Therefore, the recycling and reuse of wastewater effluents are necessary to enhance the limited fresh water supply (Qu and Fan 2010). Hence, it is essential to minimize dyes and heavy metal ions to acceptable limits before being discharged to water bodies. During the past few decades, several techniques have been realized to design feasible wastewater/water treatment technologies (Gupta et al. 2012). For example, biological treatments are designed to successfully remove various forms of pollutants from water/wastewater resources; nonetheless, this technique also usually produce secondary pollution (Ganzenko et al. 2014), as well as health-threatening bacteria, and soluble refractory organic compounds, which are difficult to remove (Ray et al. 2013). Therefore, developing green, nondestructive, and sustainable technologies for water/wastewater treatment is of much importance.

As a green, nondestructive, and promising technology, heterogeneous semiconductor photocatalysis has recently received broad interest for wastewater/water treatment owing to its effectiveness to remove harmful bacteria and pollutants (Yang et al. 2010). Mostly, the semiconductors can be photoactivated by a photon, which has an energy equal to or greater than its band gap (E_g) (Fageria et al. 2014). As a renewable and safe energy source, the solar energy is the best energy supply

needed for the activation process (Chang 2014). To effectively use the natural sunlight to handle water pollution problems, it is of significant interest to discover new visible light-driven photocatalysts.

Since the initial study by Fujishima and Honda (Fujishima and Honda 1972), several semiconductor materials, such as metal-free semiconductors (Cao et al. 2015), plasmonic metals (Sun et al. 2015), metal oxides (Li et al. 2015), metal sulfides (Zhang and Guo 2013), and metal (oxy)nitrides (Hitoki et al. 2002), are available for multifunctional and diversified applications (Wang et al. 2013d). Nevertheless, some of these semiconductor photocatalysts cannot completely satisfy the practical applications due to their short lifetime of photogenerated charge carriers and wide band gap (Li et al. 2015). Therefore, it is significant to design highly stable and efficient photocatalysts with visible light-driven activity by optimizing the existing approaches by incorporating them with nanocarbon (Zhou et al. 2014b). Recently, activated carbons with a high surface area are considered as a conventional adsorbent for water purification (Bhatnagar et al. 2013). Nonetheless, the column fouling and high production cost are the major disadvantages of using activated carbons as an adsorbent. In the last decade, graphene has been promising adsorbents for water treatment owing to its fast adsorption kinetics, excellent electronic property, large surface area, and low-cost compared to the well-developed activated carbons (McAllister et al. 2007; Xu et al. 2013b; Zhu et al. 2011). In this book chapter, much effort has been made to comprehensively review the properties, synthesis, characterization techniques, and application of graphene/semiconductor composites for the removal of water pollutants, such as organic molecules, waterborne pathogens, and heavy metal ions. The theoretical outcomes in water treatment using graphene/semiconductor composites are also summarized. A brief outlook on the challenges and new strategies is provided for developing effective water/wastewater treatment techniques using graphene-based materials.

1.2 Semiconductors Overview

A semiconductor is a crystalline structure, which has a few free electrons at room temperature (Rahman 2015). Semiconductors are the basic building block of modern electronics, such as transistors, solar cells, light-emitting diodes, analog, and digital integrated circuits (Rahman 2015). The semiconductor properties depend on the quantum physics to explain the migration of electron–hole pairs in a lattice and crystal structure (Feynman et al. 2013). A semiconductor has an electrical conductivity property between that of an insulator (e.g., glass) and a conductor (e.g., copper) (Feynman et al. 2013). Semiconductor devices show beneficial properties, such as sensitivity to heat/light and variable resistance (Rahman 2015). Semiconductors can be used for energy conversion, switching, and amplification since their electrical properties can be tuned by applying electrical fields or doping. An *n-type* semiconductor is a doped semiconductor containing free electrons, while *p-type* is a semiconductor containing free holes. Semiconductor heterogeneous photocatalysis is

mostly suited for the degradation of water/wastewater containing low concentrations of pollutants (Schneider et al. 2014). For water/wastewater purification, the oxidizing radicals can degrade the pollutants by reduction and oxidation reactions (Friedmann et al. 2010). The inherent electronic band structure of semiconductors is mostly characterized by its valence band (VB), conduction band (CB), band-gap energy, and Fermi level (Sze 2008). The VB is formed by the interactions of the highest occupied molecular orbital, while the CB is formed by the interactions of the lowest unoccupied molecular orbital. The band gap is the energy difference between the conduction band minimum (CBM) and the valence band maximum (VBM). The band structure is very important as it determines the redox ability and visible light-driven activity of semiconductor-based photocatalyst materials.

1.2.1 Basic Principles and Mechanism for Photocatalytic Pollutant Removal

A typical photocatalytic system comprises of two components: a catalytically active site and light-harvesting center to aid the pollutant degradation process (Gao et al. 2017). To enhance the activity of both components, their interactions that depend on the charge kinetics upon photoexcitation and behaviors in a photocatalytic system are of significant interest. The light-harvesting center in a heterogeneous photocatalytic system is mostly a semiconductor. The series of reductive and oxidative reactions that occur during the photocatalytic process has been widely proposed.

Under properly simulated light irradiation with photon energy greater than or equal to the semiconductor band-gap energy, electrons (e^-) and holes (h^+) are generated as shown in Eq. (1.1) and Fig. 1.1.

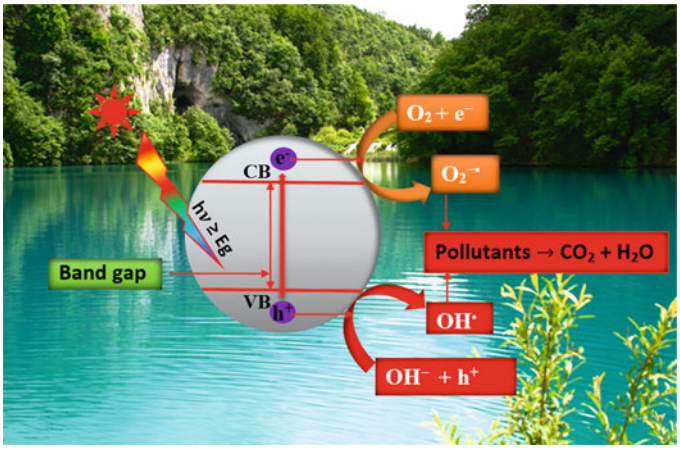

Fig. 1.1 Photodegradation mechanism of organic pollutants in water resources

$$\text{Photocatalyst} + h\nu \rightarrow h^+ + e^- \tag{1.1}$$

At the semiconductor surface, electrons then migrate from the valence band to the conduction band, forming holes (h^+) in the valence band. The three main active species that usually partake in the photocatalytic reactions are the superoxide radical anion ($O_2^{-\bullet}$), hydroxyl ($HO^\bullet$) radical, and h^+ with the $HO^\bullet$ radical as the main oxidant involved in the photodegradation of contaminant in an aqueous medium. The thermodynamics of the photocatalytic reduction and oxidation reactions are determined using the band edge positions of a given photocatalyst. Therefore, during the photodegradation reaction, it is essential to consider the reduction and oxidation potentials of the substrate and several other intermediate reactions that will occur. The electrons can combine with the oxygen (O_2) molecule to produce the $O_2^{-\bullet}$, which further forms the hydroxyl radicals only if the reaction is thermodynamically favorable (Eqs. 1.2, 1.3, and 1.5).

$$e^- + O_2 \rightarrow O_2^{-\bullet} \tag{1.2}$$

$$O_2^{-\bullet} + H^+ \rightarrow HOO^\bullet \tag{1.3}$$

$$2HOO^\bullet \rightarrow O_2 + H_2O_2 \tag{1.4}$$

$$H_2O_2 + h\nu \rightarrow 2HO^\bullet \tag{1.5}$$

Concurrently, the h^+ then interacts with water (H_2O) or hydroxyl ion (OH^-) to generate the $HO^\bullet$ radicals (Eqs. 1.6 and 1.7).

$$h^+ + HO^- \rightarrow HO^\bullet \tag{1.6}$$

$$h^+ + H_2O \rightarrow HO^\bullet + H^+ \tag{1.7}$$

The resulting $HO^\bullet$ radical serves as a strong oxidizing agent, which then combine with the organic pollutants in the water matrices to form an intermediate product, which then produces CO_2, H_2O, and other products (Eq. 1.8).

$$\text{Pollutant} + HO^\bullet \rightarrow CO_2 + H_2O + \text{Degradation product(s)} \tag{1.8}$$

Furthermore, depending on the oxidation conditions and catalyst type, the photogenerated holes are broadly regarded as an oxidant to directly degrade the organic pollutants (Chong et al. 2010). Thus, in the absence of hole or electron scavenger, the photoinduced electrons can recombine with holes after their generation. Therefore, the presence of specific scavengers is essential for restraining the charge recombination rate to enhance the photocatalytic efficiency.

To develop a semiconductor photocatalyst material capable of utilizing a wider part of the solar energy effectively, the semiconductor must have a (1) smaller band gap to absorb a broad region of the electromagnetic spectrum, (2) a favorable VB edge position for the generation of h^+ and hydroxyl radicals (Casbeer et al. 2012), (3) high stability, and (4) efficient charge separation and migration (Qu and Duan 2013).

1.2.2 Fundamentals of Semiconductor-Based Photocatalyst Materials

Thermodynamics of Heterogeneous Semiconductor Photocatalyst

Thermodynamically, the relative energy bands of graphene and semiconductors play a key role in attaining enhanced photocatalytic performance. The reduction and oxidation reactions at the semiconductor surface are driven by the photoinduced charge carriers only if their potentials straddle the CB and the VB edge positions. Thus, to achieve a high photodegradation of a given pollutant, the photoinduced holes and electrons must have a favorable oxidation and reduction ability to combine with the species adsorbed on the semiconductor surface to generate free radicals, which can act as reactive species during the photodegradation process (Chen et al. 2010). Therefore, the more positive valence band edges are helpful for an oxidation reaction, while the more negative conduction band edges are favorable for a reduction reaction. The potentials of selected species are shown in Table 1.1 (Bard et al. 1985).

Kinetics of Heterogeneous Semiconductor Photocatalyst

Generally, the thermodynamic properties, such as narrow band gap and suitable band edge positions, do not allow high performance of the semiconductor photocatalysts since the overall photocatalytic activity is affected by other factors. These include interface/surface morphology, structure at nano- and microlevels, crystallinity, composition, and adsorption capacity of the materials (Li et al. 2015). The complicated surface reaction kinetics and charge carrier dynamics in the multistep process of photocatalysis result in a low quantum yield (Pasternak and Paz 2013). The underlying mechanism of photocatalysis comprises (Pasternak and Paz 2013) (1) light harvesting, (2) charge separation, (3) charge migration/recombination, and (4) charge utilization. Kinetically, the rapid recombination rate of charge carriers is a limiting factor in achieving enhanced photocatalytic activity (Li et al.

Table 1.1 Standard redox potential for selected active species involved in the photodegradation of pollutants (Bard et al. 1985)

Reaction	E^0 (V vs. normal hydrogen electrode at pH = 0)
$e^- + O_2 \rightarrow O_2^{-\bullet}$	−0.330
$2e^- + O_2 + H_2O \rightarrow HO_2^- + OH^-$	−0.065
$e^- + O_2 + H^+ \rightarrow HO_2^\bullet$	−0.046
$e^- + HO_2^- + H_2O \rightarrow HO^\bullet + OH^-$	0.184
$e^- + O_2^- + H_2O \rightarrow HO_2^- + OH^-$	0.200
$2e^- + O_2 + 2H^+ \rightarrow H_2O_2$	0.695
$4h^+ + 2H_2O \rightarrow O_2 + 4H^+$	1.229
$h^+ + OH^- \rightarrow HO^\bullet$	2.690
$4h^+ + 4OH^- \rightarrow O_2 + 2H_2O$	0.401

2015). Moreover, the agglomeration of nanostructured particles and the low specific surface area not only increases the diffusion barriers of the reagents but also decreases the surface oxidation and reduction kinetics, which reduces the photocatalytic performance. Thus, several factors, such as surface reaction kinetics, charge carrier kinetics, diffusion, and adsorption, are kinetically significant in designing highly efficient photocatalyst materials.

1.3 Factors Controlling Photocatalytic Pollutant Removal

A major concern with the heterogeneous photocatalytic process for organic synthesis by oxidation is the highly oxidizing environment and non-selectivity, with products being lost due to complete mineralization. Although semiconductor photocatalysts have potential applications, they still have unwanted disadvantages, such as the wide band gap that limits wider use of solar energy, large interfacial area that induces slow charge carrier migration, nanoscale features, and single phase that causes fast recombination of photogenerated charge carriers. Their effectiveness to the photocatalytic reaction is influenced by factors (Friedmann et al. 2016), such as the excitation of charge carriers from the bulk to the surface, as well as the separation/recombination of charge carriers that occurs in the bulk or at the surface. Besides the band structures and diffusion kinetics, other factors, such as surface properties, crystallinity, morphological architecture, and material choice, must be considered when designing stable and efficient visible light-driven photocatalytic materials (Mori and Yamashita 2010). Thus, choosing the right semiconductor is quite significant, because it determines the visible light photocatalytic performance (Yan et al. 2014). Moreover, the right morphological architecture between the redox reaction center and the photogenerated charge carriers junction can effectively enhance the separation and migration of charge carrier (Yan et al. 2014). The high degree of crystallinity with crystal defects will minimize the recombination rate at the interface, thereby enhancing the efficiency of the photoinduced charge carriers to partake in the redox reaction (Gu et al. 2014). The surface area, which relies on the geometrical shape and porosity of the photocatalysts, influences the photocatalytic performance (Zhu et al. 2010). The adsorption capacity of the semiconductor photocatalysts toward pollutant degradation increases if there are more atoms present on the surface. The absence of well-designed porous interconnected network assembly at larger length scales may unfavorably affect the overall photocatalytic performance.

1.4 Characterization of Nanomaterials

To show the behavior of charge carriers in the photocatalytic material, it is vital to analyze the charge kinetic via several characterization techniques with emphasis on spectroscopic techniques. Currently, several characterization techniques have been

developed to check the charge kinetics behavior at the photocatalysis process. Explicitly, the photogenerated charge carriers are examined by characterizing the band structure and light absorption. Based on charge separation and migration, the characterization techniques are mostly concentrated on charge dynamics (photoexcited charge carrier separation and lifetime efficiency). Moreover, several advanced techniques have been widely designed to check surface reactions, such as the molecular desorption/adsorption, reaction paths, reactant dissociation, and intermediate product.

1.4.1 Charge Carrier Transfer Kinetics

Besides charge transfer kinetics, the charge separation, migration, and recombination processes normally occur in an ultra-small timescale. The transient absorption spectroscopy, which measures the signals for charges at the ground/excited state, and the recombination rate of photogenerated charge carriers, has been broadly utilized in a photocatalytic mechanism study (Berera et al. 2009). However, transient absorption spectroscopy cannot fully reflect the photocatalytic process under simulated solar light irradiation owing to the robust pulsed laser used as excitation sources (Berera et al. 2009). Therefore, photoelectrochemical measurements have been used to check the charge kinetics behavior and average dynamic parameters of a photocatalytic system (Sato 1998). Moreover, the recombination of photogenerated carriers is measured by the time-resolved/steady-state photoluminescence spectroscopy (Anpo and Kamat 2010). Generally, the low intensity in the steady-state photoluminescence spectroscopy shows a low chance of recombination rate of charge carrier. For time-resolved photoluminescence spectroscopy, a rapid photoluminescence degeneration with a short lifetime shows a low recombination of electrons with holes.

1.4.2 Band Structure and Light Absorption

Ultraviolet-visible diffuse reflectance spectroscopy is used to quantify the optical band gaps of semiconductors and light absorption of semiconductor photocatalyst materials. In contrast to ultraviolet-visible spectroscopy, the synchrotron-based soft X-ray spectroscopy is used to measure the electronic structure of complex materials, wherein the VBM and CBM are measured by the X-ray emission and absorption spectroscopy, respectively (Kapilashrami et al. 2014). Synchrotron radiation-based X-ray spectroscopy provides the ability to analyze the band structure of photocatalyst materials, while modifying the wavelength of the incident light allows the study of element-selective photocatalyst materials (Vayssieres 2010).

1.4.3 Surface Reaction

Upon obtaining the charge transfer kinetics and band structures, an in-depth insight of charge dynamics in the photocatalytic reaction on the semiconductor surface is vital for completing the photocatalyst design (Osgood 2006). To measure the surface reaction, several characterization techniques have been established as powerful tools to detect the reaction pathways, products, and intermediate, as well as the activation and adsorption sites of the redox reaction. Infrared (IR) spectroscopy is widely used to check surface reactions. Explicitly, the Fourier transform IR spectroscopy is used to investigate the nature of adsorbed species and the surface properties of photocatalyst systems (Chen et al. 2007). Separately, time-resolved infrared spectroscopy can precisely measure the charge kinetics of the adsorbed species (Chen et al. 2007). Thermal desorption spectroscopy (TDS) is used to measure the thermodynamic and kinetic reaction of desorption and adsorption processes on the photocatalyst surface (Yuan et al. 2013). The defect sites on the photocatalyst surface can be measured by electron spin resonance spectroscopy, X-ray absorption spectroscopy, X-ray absorption fine structure, and positron annihilation spectroscopy (Bai et al. 2015).

1.5 Synthesis of Nanomaterials

Up to now, several semiconductor heterostructures have been successfully designed and synthesized. Mostly, the three-dimensional nano−/microcomposites are synthesized via the self-assembly of nanosized building blocks, such as nanowires, nanosheets, and nanoparticles (Li et al. 2016). Nonetheless, it is extremely challenging to design and synthesize several types of photocatalyst materials with controlled morphologies. Therefore, it is essential to design a simple and low-cost technique to prepare photocatalyst materials with hierarchical and high crystallinity nanostructures. Up to now, hierarchical semiconductor photocatalysts are prepared via template-free methods (chemically induced self-transformation, self-template strategy, and in situ template-free assembly), template method (in situ template-sacrificial dissolution and two-step template method), and post-synthetic treatment method (Li et al. 2016). The template method is one of the most often used technique to fabricate hierarchical nanostructured photocatalysts due to its good reproducibility, abundant types of physical templates, and large-scale synthesis (Liu et al. 2013b). The in situ template-sacrificial dissolution technique has drawbacks, such as the high cost of template, the presence of heterogeneous impurities, tedious synthetic procedures, and sudden morphological changes during template removal (Li et al. 2016). All these limit the large-scale synthesis of photocatalyst materials (Lou et al. 2006). The self-template method is among the most effective and simple techniques to synthesize several photocatalyst materials (Cai et al. 2009). The

chemically induced self-transformation (Qi et al. 2016) method has been used to synthesize several hierarchical hollow microspheres, such as $CaCO_3$, TiO_2, Al_2O_3, SnO_2, and WO_3. The mechanism of the in situ template-free assembly differs from the chemically induced self-transformation (Li et al. 2016). The chemically induced self-transformation involves the creation of hollow interiors through chemical etching of the primary particles, while the in situ template-free assembly involves the self-assembly of nanosized building blocks around the nuclei (Yu et al. 2006).

1.6 Graphene

Nanomaterials with unique properties can be used to design new technologies, as well as improving the performance of existing processes due to their nanoscale dimensions. Nanomaterials have been used to solve major environmental issues, such as contaminant sensing, energy production, and water treatment (Qu et al. 2013). The latest nanomaterials to capture the interest of researchers is graphene (GR), which is a two-dimensional (2D) layer of carbon (C) atoms arranged in a honeycomb crystalline structure (Geim 2009). The interest is due to its unique and notably exceptionally large surface area, physicochemical properties, excellent mechanical strength, thermal and electron mobility.

1.6.1 History of Graphene

Graphene is a thin layer hexagonal crystal structure comprising a 2D monolayer planar sheet of sp^2-bonded C atoms. Graphene is the building block of graphite with the π-stacking sheets holding the lamellar graphite structure (Hontoria-Lucas et al. 1995). The interlayer spacing between the sheets was recorded at 3.34 Å (Hontoria-Lucas et al. 1995). Through a micromechanical cleavage route, graphene was initially synthesized from graphite (Novoselov et al. 2004). This method permits easy fabrication of high-quality GR crystallites, which can lead to massive experimental process (Katsnelson 2007). Under ultrahigh vacuum (<1010 torr) and elevated temperatures, monolayer flakes of carbon with graphene structure were obtained via the epitaxial sublimation of silicon from silicon carbide (SiC) monolayer (Van Bommel et al. 1975). The term "graphene" was described as a single-atom carbon sheet by Boehm et al. (1986). This graphene sheet showed a transparent, flat, and monolayer sheetlike honeycomb structure comprising a single layer of sp^2-bonded C atoms with a C–C bond length of 1.42 Å. The 2D crystals of graphene were thermodynamically unstable under ambient conditions (Yusuf et al. 2015). However, Novoselov et al. (2004) successfully isolated and characterized a mechanically exfoliated graphene monolayer.

1.6.2 Properties and Structure of Graphene

Graphene is a zero band-gap semiconductor, and its unique electronic properties show a low absorption ratio of 2.3% of light and an unpredictably high cloudiness of atomic monolayer (Kuzmenko et al. 2008). Fundamentally, graphene shows fascinating properties, such as high charge carrier mobility (100,000 $cm^2\ V^{-1}\ s^{-1}$), large surface area (2630 $m^2\ g^{-1}$), Young's modulus (~1100 GPa), high thermal conductivity (2000–5000 $W\ m\ K^{-1}$), large electric current density ($10^8\ A\ cm^{-2}$), and superb mechanical strength (2.4 ± 0.4 TPa) (Upadhyay et al. 2014). These unique properties makes graphene an interesting material for several applications in liquid crystal devices, solar cells, capacitors, sensors, batteries, and water treatment (Upadhyay et al. 2014). Graphene is the basic building blocks for several C allotropes, such as fullerenes (0 D), graphite (3 D), and carbon nanotubes (1 D) (Fu and Wang 2011a). Two sub-lattices of C atoms in the graphene lattice are linked with the s and p orbitals of each C atom in the lattice, and this contributes to the electron delocalization network. Graphene's structure is defect-free since similar types of atoms are bonded by flexible and strong bonds, which contributes to the extraordinary properties of graphene.

1.6.3 Synthesis of Graphene

Using a Scotch tape, graphene was initially prepared using the manual mechanical cleavage of graphite (Novoselov et al. 2004), and since then several synthetic techniques have been reported (Allen et al. 2009). These techniques are the bottom-up and top-down methods (Allen et al. 2009). The bottom-up method is the direct fabrication of graphene from molecules or atoms through chemical reactions. Some typical examples of the bottom-up methods includes chemical vapor deposition (CVD) on the surface of metal foil, solvothermal, organic synthesis, and epitaxial growth on single crystals of silicon carbide (Emtsev et al. 2009). However, the bottom-up approaches are not broadly used owing to their high cost and complexity of the substrates. Currently, high-quality GR sheet with a distinct molecular structure has been fabricated by the top-down approaches, such as electrochemical synthesis (Guo et al. 2009), unzipping of carbon nanotubes (Jiao et al. 2010), chemical exfoliation of graphite (Park et al. 2009), arc discharge (Subrahmanyam et al. 2009), micromechanical cleavage (Schedin et al. 2007), liquid phase exfoliation of graphite (Zhou et al. 2014a), thermal exfoliation (McAllister et al. 2007), electrostatic deposition (Tung et al. 2009), and chemical reduction of graphene oxides (Compton and Nguyen 2010). The synthesis techniques of graphene for environmental remediation application must be simple, efficient on a large scale, and cost-effective. However, not all these techniques are possible for water/wastewater treatment. Up to now, there have been a few reports on the fabrication of pristine graphene for water/wastewater treatment. Through a facial

liquid phase exfoliation, Li et al. (2011b) synthesized a monolayer graphene sheet from wormlike graphite. The as-synthesized graphene was utilized to adsorb fluoride from aqueous solution after 1-methyl-2-pyrrolidinone was removed at 200 °C. The epitaxial growth technique of graphene can be realized by heating a honeycomb crystals of SiC at 2400 K (McAllister et al. 2007). For example, the vacuum graphitization technique was used to fabricate epitaxial graphene via the thermal decomposition of SiC at 2400 K (Berger et al. 2006). The mechanical exfoliation method was the first method used for the synthesis of graphene (Novoselov et al. 2004). In this method, an extremely oriented pyrolytic graphite was entrenched in photoresist materials, and the graphene layers were peeled off using adhesive tape. Recently, the Hummers' method/modified Hummers' method is found as the most highly and commonly used technique (Hummers and Offeman 1958). In this method graphite is oxidized into graphene oxide using strong acids (e.g., $KMnO_4$ and H_2SO_4) to form a stable graphene oxide solution dispersed in water (Some et al. 2012), which are then reduced using hydrazine (Li et al. 2008). The CVD method was used to fabricate graphene using a metal substrate under high temperature and ultrahigh vacuum (Tung et al. 2009). In this process, graphene was deposited on the metal substrate surface, such as Cu and Ni with a vapor-rich hydrocarbon heated at ~1073 K. Liquid-phase exfoliation of graphite oxide is among the most practical methods for industrial fabrication of GR owing to its low-cost and scalability (Zhou et al. 2014a). This process encompasses the sonication of graphite oxide/graphite powders in aqueous solution.

1.6.4 Characterization of Graphene

The identification of graphene monolayers is a major issue faced during the characterization of graphene. Up to now, several techniques including the X-ray diffraction, scanning electron microscopy, thermogravimetric analysis, Raman spectroscopy, Fourier transform infrared spectroscopy, transmission electron microscopy, X-ray photoelectron spectroscopy, and atomic force microscopy have been used to characterize graphene. Since it is difficult for a single technique to offer all the essential information, there is the need to combine two or more tools to precisely characterize the intrinsic properties, texture, morphology, and crystal structure of graphene (Guo and Dong 2011). Transmission electron microscopy (Hernandez et al. 2008) images was used to measure the thickness and the number of graphene sheets. Raman spectroscopy analysis is a nondestructive technique, which uses monochromatic laser excitation to investigate the structure of graphene (Machado and Serp 2012). There are three response peaks (D peak = ~1350 cm^{-1}, 2D peak ~2700 cm^{-1}, and G peak = ~1580 cm^{-1}) equal to different phonon/vibrational modes in graphene (Ferrari et al. 2006). The D peak appears strongly in disorderly graphite, which indicates the degree of graphene disorder. Based on the position, shape, and width of the 2D peak, the quality and number of graphene layers can be investigated using Raman spectroscopy (Ferrari et al. 2006). The crystalline structure of graphene sheets is determined

using X-ray diffraction. The diffraction peak of graphene is linked to the A–B stacking order, which correlated with the [002] reflection (Machado and Serp 2012). The [002] reflection occurred at $2\theta \approx 26^\circ$ for pristine graphite, and after oxidation, the layers were shifted to $2\theta \approx 11^\circ$ (Machado and Serp 2012). The number of layers is evaluated using the line broadening by the Lorentzian fitting of the [002] reflection and the Scherrer equation (Rao et al. 2009). Currently, atomic force microscopy is among the most effective technique used to detect few-layer and single-layer crystals (Blake et al. 2007). Therefore, the atomic force microscopy can measure elastic, magnetic, electrical, and mechanical properties of graphene (Singh et al. 2011). The scanning electron microscopy images are used to determine the presence of defects and morphology of graphene, as well as acquiring atomically resolved images of graphene sheets (Machado and Serp 2012).

1.6.5 Adsorption Mechanism of Graphene

The adsorption properties of graphene are influenced by surface properties, such as distribution, surface area, and pore size (Yusuf et al. 2015). Thus, the surface area largely influences the adsorption of adsorbate on the adsorbent since the surface area per unit volume of the adsorbate determines the adsorption ability of the adsorbent (Yusuf et al. 2015). During the adsorption process, a larger surface induces a large surface area of active sites exposed to the adsorbate (Yusuf et al. 2015). Hence, an adsorbent with a small grain size distribution and high porosity increases the adsorption ability and the total surface area (Mohanty et al. 2008). However, graphene exhibited no porosity and an ultrahigh specific surface. The adsorption capacity of graphene can be enhanced by combining with other porous materials (Zhang et al. 2011a).

1.7 Progress on Graphene and Semiconductor Composites

There has been much interest in the fabrication of graphene/semiconductor composites due to the variety of functional semiconductor nanoparticles (Lü et al. 2012). During the pollutant removal process, graphene can often tune the properties of semiconductors. In particular, magnetic Fe_3O_4 nanoparticles have been used as magnetic separation in large-scale industrial application and to address several problems related to gravitational separation, filtration, and centrifugation of graphene. Coupling graphene with a semiconductor is an attractive material for photocatalytic applications since graphene has a zero band gap, high conductivity of electron in storage, and migration of electrons. The nanoparticles on the graphene surface prevent the aggregation of GR sheets to some degree in the composites, which further increases the exposed area for the elimination of pollutants from water/wastewater resources.

1.7.1 Graphene/Semiconductor Composites as Adsorbents

Rapid population growth, industrial, and agricultural activities have given rise to a large number of contaminants being released into the environment, which represent a major public health and environmental concern (Lubchenco 1998). Heavy metal pollutants from municipal waste, industrial waste, corrosion of pipes, and soldered joints are common contaminants that can unpleasantly enter drinking water sources and aquatic environments (USEPA 2014). Therefore, much effort has been made to develop a technology, which can effectively remove pollutants from water. Among them, adsorption is the most effective technology for water/wastewater treatment owing to its inexpensive, low-cost, and efficacy for pollutant removal from aquatic environments (Ali and Gupta 2006). Adsorption involves the capturing of pollutants (adsorbate) by nanomaterials (adsorbents) through a physicochemical interaction (Dąbrowski 2001). Ideally, graphene with a large surface area (2630 $m^2\ g^{-1}$) makes it an attractive adsorbent for the decomposition of pollutants (Ramesha et al. 2011) compared to the conventional adsorbents, such as mesoporous and activated carbons. Moreover, the large π–π conjugation on the surface of graphene could be used for the adsorption of different reactants during the photocatalytic reaction. Moreover, the semiconductor has a large surface-to-volume ratio. Therefore, coupling a graphene sheet with a semiconductor can effectively improve the adsorption capacity and surface area of the composite. Graphene/magnetic nanoparticle composites exhibited enhanced adsorption activity and improved the number of binding sites for heavy metal ions and the surface area of the nanoparticle (Zhu et al. 2011). This is due to the combined effect of adsorption sites on the graphene layer and the metal complexation on the nanoparticles (Zhu et al. 2011). Among the magnetic semiconductor, Fe_3O_4 is the most used semiconductor for water purification owing to its extraordinary biocompatibility (Chandra et al. 2010). Higher conductivity and surface area influence the deionization activity of semiconductors (Wang et al. 2013a). Fortunately, graphene shows both properties, which makes it suitable for the deionization of semiconductors (Zhang et al. 2012a). Wang et al. (2012a) observed a reduction in conductivity from 86.9 to 10.2 μS cm^{-1} after 120 min when graphene was used as an electrode for the deionization of sodium chloride solution. The magnetic graphene/Fe_3O_4 nanocomposites, which was fabricated using a facile one-pot technique, was utilized as an adsorbent to eliminate rhodamine B (RhB) dye from wastewater (Lü et al. 2014). The as-fabricated nanocomposite displays high ability to extract organic pollutants. Thus, the magnetic graphene/Fe_3O_4 adsorbent allows efficient separation of pollutants from wastewater. Zhu et al. (2011) revealed that a complete removal of Cr(IV) by the magnetic graphene composite in acidic pH ranges from 1 to 3. Similarly, a high acidic pH solution can also inhibit the adsorption ability of metal ions by the composites (Alyüz and Veli 2009). The Fe_3O_4/graphene composite with the covalent binding between graphene and Fe_3O_4 showed high adsorption capacity of 190.14 and 140.79 mg g^{-1} for methylene blue (MB) and neutral red dyes, respectively (He et al. 2010). Through a chemical reduction process, a magnetic Fe_3O_4/graphene

composite was fabricated and used to remove Congo red and MB dyes from wastewater media (Yao et al. 2012). The magnetic iron composite showed enhanced adsorption capacities of 33.66 and 45.27 mg g^{-1} for Congo red and MB dyes, respectively. Thus, the composite had a high potential as an efficient adsorbent for removing dyes from aqueous solution. A magnetic nanocomposite was reported to have a high adsorption of fuchsine dye with about 96% of fuchsine dye adsorbed (Wang et al. 2011a). This enhanced adsorption was due to the van der Waals interactions between the honeycomb packed C atoms and the aromatic backbone of fuchsine dye molecule, as well as the delocalized π-electron of the graphene sheet and the π–π stacking interactions of the aromatic part of fuchsine dye. A magnetic $CoFe_2O_4$/graphene composite was prepared by the hydrothermal treatment of exfoliated GR monolayers and inorganic salts (Li et al. 2011a). The as-prepared nanocomposites showed adsorption high capacity (71.54 mg g^{-1}) to effectively remove methyl orange (MO) dye. The SiO_2/graphene composite, which was fabricated via a two-step technique, exhibited a high adsorption capacity (113.6 mg g^{-1}) toward Pb^{2+} ion removal with reference to divalent ions, such as Cd^{2+}, Ni^{2+}, Co^{2+}, Cu^{2+}, and Cr^{3+} (Hao et al. 2012). Nonetheless, the adsorption capacity of SiO_2/graphene composite was suppressed by the addition of KNO_3. The effect of hydrothermal treatment period on the adsorption performance of TiO_2/graphene composite was investigated by Lee and Yang (2012) for the effective elimination of Pb^{2+}, Cd^{2+}, and Zn^{2+} ions. They found that the exposure area of the composite was improved from 88.97 to 132.74 m^2 g^{-1} and the adsorption capacity from 45.0 ± 3.8 to 65.6 ± 2.7 mg g^{-1} for Pb^{2+}, 44.8 ± 3.4 to 88.9 ± 3.3 mg g^{-1} for Zn^{2+}, and 65.1 ± 4.4 to 72.8 ± 1.6 mg g^{-1} for Cd^{2+} upon prolonging the hydrothermal treatment period from 6 to 12 h. A graphene nanosheet/Fe_3O_4 composite, which was synthesized by a facile one-step solvothermal route, showed fast adsorption rates and excellent removal capacity of MB dye in water (Ai et al. 2011). This enhancement was ascribed to the π–π interaction between the aromatic ring of graphene and the MB dye, as well as electrostatic attraction between the cationic MB and the negative surface of oxygen-containing groups. This study shows that the as-synthesized composite could be used as efficient adsorbents for water purification. A detailed investigation of the δ-MnO_2/graphene composite before and after adsorption of lead and copper ions was performed by Ren et al. (2012), and they found that the metal ions not only interpolate in the interlayer of δ-MnO_2 but also get adsorbed on the composite surface. Moreover, the δ-MnO_2/graphene composite displayed high cycling, and the as-prepared composite can be utilized for at least four times, without any significant loss in the adsorption capacity. The adsorption of Ni ions on graphene/δ-MnO_2 composite showed enhanced adsorption capacity from 46.55 to 60.01 mg g^{-1}, and this was 15 and 1.5 times higher than graphene nanosheets and δ-MnO_2, respectively (Ren et al. 2011).

A graphene-based Fe_3O_4 magnetic nanoparticle was used as adsorbent for magnetic solid-phase extraction of prometon, atrazine, prometryn, and propazine (Zhao et al. 2011). They established that the adsorbent was efficiently removed from aqueous solution by an external magnet. A magnetic graphene/Fe_3O_4 nanocomposite, which was fabricated by chemical precipitation method, had been

used as a novel adsorbent for the preconcentration of carbofuran, metolcarb, pirimicarb, diethofencarb, and isoprocarb (Wu et al. 2011b). The as-fabricated nanocomposite showed excellent super paramagnetic properties and adsorption capacity. A magnetic microsphere Fe_3O_4/SiO_2/graphene composite was fabricated as a new adsorbent for the preconcentration of di-*n*-propyl-phthalate, diallyl phthalate, dicyclohexyl phthalate, benzyl butyl phthalate, and diethylhexyl phthalate in soybean milk and water samples (Wang et al. 2013c). The Fe_3O_4/graphene nanocomposite prepared by solvothermal route effectively removed aniline from their aqueous solution within 60 mins (Chang et al. 2012). The composites showed a promising adsorbent for phthalate esters with potential applications. A magnetic Fe_3O_4/graphene composite was used for the extraction of some sulfonamides (sulfamerazine, sulfapyridine, sulfamonomethoxine sodium, sulfameter, sulfadoxine, and sulfachloropyridazine) from the water (Luo et al. 2011). The composite exhibited efficient extraction media for the enhancement of sulfonamide antibiotics in water resources.

1.7.2 Graphene-Based Photocatalyst Materials for Water Treatment

Although adsorption can eliminate pollutants from water/wastewater, this method cannot completely remove pollutants (Chong et al. 2010). Complete mineralization of pollutants can be achieved through a photocatalytic technique (Chong et al. 2010). Recently, semiconductor photocatalyst materials have received global interest in water remediation application (Hoffmann et al. 1995). Nonetheless, the fast recombination of charge carriers results in a low quantum efficiency, which limits its potential visible light applications. Hence, reducing the recombination rate of charge carriers is significant to enhance the photoactivity of semiconductor photocatalysts. The most significant characteristics of graphene sheet for photodegradation of pollutants are due to its ability to tune the band gap and absorption edge of semiconductor photocatalyst materials. The ultrahigh electron conductivity of GR allows the transfer of electrons from the semiconductor to the graphene surface, and this contributes to the reduced recombination rate, thus improving the photocatalytic activity of conventional photocatalysts, such as TiO_2 (Liu et al. 2010). Therefore, composites that combine semiconductor photocatalysts and graphene might offer a desired efficiency for separating the charge carriers. Due to its strong oxidizing activity and low-cost, TiO_2 is the most often used semiconductor for the photodegradation of pollutants. The popularity of TiO_2 is explained by its commercial availability, such as P90 and P25, which serves as reference reagents for the fabrication of graphene-based TiO_2 photocatalyst composites (Liu et al. 2010). Coupling graphene sheets with TiO_2 improved the photoactivity of the composites. Apart from TiO_2, several metal oxides, such as WO_3 (An et al. 2012), ZnO (Min et al. 2012), CuO (Yusoff et al. 2013), Cu_2O (Gao et al. 2012a), SnO_2 (Seema et al.

2012), Mn_2O_3 (Chandra et al. 2012), $BiVO_4$ (Yan et al. 2013), $ZnWO_4$ (Bai et al. 2012), Bi_2WO_6 (Gao et al. 2011), Bi_2MoO_6 (Wang et al. 2012b), $CoFeO_4$ (Fu et al. 2012), and $BaCrO_4$ (Gawande and Thakare 2013), have been used in combination with graphene to serve as a photocatalyst. Theoretically, these semiconductor photocatalysts are characterized by their electronic band structure, which composes of an empty CB and filled VB (Xiang et al. 2012). The P25/graphene nanocomposites, which was fabricated using the hydrothermal route exhibited a higher capacity to degrade MB dye compared to pure P25 nanoparticles (Zhang et al. 2009). The graphene sheet enhances the ability to adsorb organic contaminants, as well as improving the charge separation/migration rate, and visible light absorption of P25/graphene nanocomposites (Zhang et al. 2009). Coupling a semiconductor with graphene reduces its band gap through the hybridization of O *np* (n = 2, 3, 4, 6, 7) and C *2p* atomic orbitals to form a new VB (Li et al. 2013a). The amount of graphene loading to the semiconductor should be carefully tuned to achieve efficient photocatalyst–support interaction. Hence, the amount of graphene sheets plays a significant role in the photocatalytic activity of the composites. Generally, increasing the graphene sheet content in composites enhances the photocatalytic performance but beyond the permissible limit reduces the photocatalytic performance (Yoo et al. 2011). The graphene/TiO_2 composite, which was prepared using the in situ method showed 2.5 times improved photocatalytic degradation of MB dye with reference to Degussa P25 TiO_2 (Wang et al. 2010). When the graphene content was increased to 20% in the $ZnFe_2O_4$/graphene composite, a higher degradation of MB dye was observed compared to $ZnFe_2O_4$ (Fu and Wang 2011b). Through a hydrothermal reaction of CeO_2/TiO_2 nanoparticles with graphene oxide in ethanol, a CeO_2/TiO_2/graphene nanocomposite was prepared (Ghasemi et al. 2012). The performance of CeO_2/TiO_2/graphene nanocomposites decreases with an increase in the graphene sheet content. The CeO_2/TiO_2/graphene composite exhibited high photocatalytic activity compared to the CeO_2/TiO_2/carbon composite owing to the unique electronic and structural properties of the graphene sheet. The influence of graphene loading on the photocatalytic performance of TiO_2/graphene composite showed that a 0.05 threshold weight percent (wt%) of graphene exhibited the maximum activity (Wang et al. 2012c). Using reduced graphene oxide and titanium isopropoxide as Ti-precursors, a series of graphene/TiO_2 composites were fabricated by a sol–gel route (Liu et al. 2013a). The as-fabricated composite showed improved degradation of MB dye compared to pure TiO_2 with graphene/TiO_2 composite exhibiting a higher activity than that of graphene/TiO_2(P25). Through a facile sonochemical approach, the Ag_2Se/graphene/TiO_2 composite was fabricated (Meng et al. 2012). The as-prepared composites demonstrated improved visible light absorption, high adsorptivity of RhB dye, and excellent separation of charge carriers. The high performance was ascribed to the synergetic effects of the absorption edge in the visible light region and high charge carrier mobility of Ag_2Se/graphene/TiO_2 composite. Khalid et al. (2012a) prepared a composite of Fe-doped TiO_2 with graphene toward the photocatalytic degradation of MO dye. Due to the reduced charge carrier recombination, the synergistic effect of enhanced adsorptivity of MO dye, and improved visible light absorption, the as-synthesized showed tenfold photocatalytic

performance compared to the bulk TiO_2. Min et al. (2013) successfully fabricated N-TiO_2/graphene composite for the photocatalytic decomposition of benzoic acid. The as-fabricated composites showed high photocatalytic activity over pristine TiO_2. The photodegradation activity of MB dye by TiO_2/graphene is two and six times faster than that of TiO_2/graphene oxide and P25, respectively (Ismail et al. 2013). This improvement was ascribed to the effective charge transfer from TiO_2 to graphene layers, as well as the better contact between TiO_2 and graphene. The good contact of graphene with TiO_2 nanoparticles enhances the photoelectron conversion of TiO_2 by reducing the charge carriers' recombination rate (Guo et al. 2011). Through, the hydrothermal process, novel graphene/TiO_2 composite efficiently photodegrades MO dye over pure TiO_2 (Khalid et al. 2013a). The efficient charge separation due to the 2D planar structure and π-conjugation system of graphene, as well as the high adsorptivity of MO dye, influences the enhanced performance of the composite. The TiO_2/graphene composite nanosheets, which was fabricated via a facile one-pot solvothermal route, showed improved adsorption capacity and much enhancements toward the photocatalytic decomposition of MB dye compared to P25 (Zhang et al. 2012c). The superiority of graphene sheets compared to carbon nanotubes toward the photocatalytic activity of TiO_2 was investigated (Zhang et al. 2011c). Comparison between carbon nanotubes/TiO_2 and graphene/TiO_2 reveals the prominent advantage of graphene over carbon nanotubes on both enhancing the photocatalytic activity and controlling the morphology of TiO_2. Using a sol–gel method, Fe-doped TiO_2 photocatalyst nanowire arrays were embedded on the surface of functionalized graphene sheets (Farhangi et al. 2011). The photocatalytic performance improved with increasing the Fe-doping concentration between 0.6 and 0.8% of Fe. The as-fabricated composites exhibited high a photodegradation of 17β-estradiol over Fe-doped TiO_2 and TiO_2/functionalized graphene sheet composites. Moreover, surface modification of graphene/semiconductor composite with metal ions, such as Au (Wang et al. 2013b), Pt (Neppolian et al. 2012), Nd (Khalid et al. 2013b), Ag (Tang et al. 2012), and Fe (Khalid et al. 2012a), can enhanced their photocatalytic performance. These metals can enhance the lifetime of charge carriers by restraining their recombination rate. Wang et al. (2013e) revealed that coupling SnO_2 with graphene promoted the performance of SnO_2 for the photodegradation of pendimethalin. This improvement was ascribed to the excitation of an electron from pendimethalin at the excited states to SnO_2 at the interface and the large potential difference between SnO_2 and pendimethalin. The underlying mechanism behind the photocatalytic performance of ZnO/graphene sheet composite was investigated by Xu et al. (2011). They observed that the presence of $O_2^{-\bullet}$, OH, and h^+ active species is responsible for the photocatalytic decomposition toward methylene blue dye. Li and Cao (2011) observed that the ZnO/graphene composite revealed a high photoactivity toward the decomposition of RhB dye. The incorporation of graphene on the semiconductor surface promotes the performance and stability of the semiconductor photocatalysts by reducing their photo-corrosion (Fan et al. 2012). The photocatalytic activity of a semiconductor is influenced by the morphology of the photocatalyst. One-dimensional WO_3/graphene nanorod composites exhibited three

times an improvement in the photocatalytic performance compared to the commercial WO_3 (An et al. 2012). Gao et al. (2011) observed a threefold increase in the performance of Bi_2WO_6/graphene composite toward the degradation of RhB dye compared to pure Bi_2WO_6. This improvement is due to the Fermi energy level shift and efficient transfer of photoinduced electrons at the Bi_2WO_6/graphene interface. The visible photocatalytic activity of $ZnWO_4$ hybridization with graphene sheet was attributed to the efficient transfer of charge carriers at the $ZnWO_4$/graphene interface (Bai et al. 2012). Moreover, carbon free radicals, which was found along with the $O_2^{-\bullet}$ and $HO^{\bullet}$ radicals, did not directly partake in the photodegradation reaction but to some degree enhanced their lifetime for the oxidative reactions. Zhang et al. (2011b) showed 1.87 times photocatalytic performance of $InNbO_4$/graphene compared to pure $InNbO_4$ for the degradation of MB dye. Iron nanoparticles/graphene composites, which was successfully fabricated using graphene oxide as a supporting matrix, showed a higher elimination capacity to decolorize methylene blue dye (Guo et al. 2012). The graphene/Mn_2O_3 nanocomposite with a uniform distribution of Mn_2O_3 nanoparticles throughout the surface of graphene sheet showed ~60, ~80, and ~84% degradation of RhB, eosin, and MB dyes, respectively (Chandra et al. 2012). The graphene/Cu_2O composites, which were fabricated at room temperature using a one-pot solution route, altered the surface charge of the composites from positive to negative (Gao et al. 2012a). This favors the adsorption and photocatalytic degradation of MB dyes under simulated visible light irradiation. Through a simple solvothermal route, graphene/CdS composite was fabricated (Gao et al. 2012b). The as-fabricated composites showed an effective migration of photoinduced electrons from CdS to graphene sheet, as well as enhanced visible light photodegradation activity for RhB dye degradation. The CeO_2/TiO_2/graphene composites synthesized by the sol–gel process exhibited a higher photocatalytic degradation of 2,4-dichlorophenoxyacetic acid and Reactive Red 195 dye in aqueous solution (Ghasemi et al. 2012). A $BiVO_4$/graphene composite was fabricated via a one-step hydrothermal route (Fu et al. 2011). The as-fabricated composite showed enhanced photoactivity for the decomposition of MO, RhB, MB, and active black BL-G dyes in water. This improvement was attributed to the effective separation of charge carriers and the concerted effects of pure $BiVO_4$ and graphene sheet. Through a hydrothermal method, copper oxide was effectively decorated with functionalized graphene sheets (Yusoff et al. 2013). Due to the enhanced synergy interactions between copper oxide and functionalized graphene sheets, the nanocomposite demonstrated higher photoactivity toward the degradation of MB dye. The SnO_2/graphene and Cu_2O/SnO_2/graphene nanocomposites fabricated by simple sol–gel growth route showed a higher photodegradation of pendimethalin than pure SnO_2 and pristine graphene (Wang et al. 2013e). The novel graphene/Sb_2S_3 composites prepared using a facile solvothermal method revealed improved photodegradation activity toward RhB dye due to the negative surface charge, efficient electrons transfer from Sb_2S_3 to the graphene sheet, and smaller Sb_2S_3 particles size (Tao et al. 2013). Within the two-step hydrothermal approach, the La-TiO_2/graphene composites have better charge separation ability and enhanced photodegradation of MB dye with reference to pure TiO_2 (Khalid et al. 2012b). The high performance

was ascribed to the higher adsorptivity of the MB dye, excellent electrical properties of graphene, increased charge separation efficiency, more π–π interactions between the composite and the pollutants, as well as the large surface contact between La-TiO_2 nanoparticles and graphene. The particle size, graphene contents, and targeted pollutants for the different graphene/semiconductor composites are presented in Table 1.2.

Table 1.2 Graphene and semiconductor composites for photocatalytic degradation of pollutants

Graphene composites	Particle size (nm)	Graphene contents (wt.%)	Pollutants	References
TiO_2/graphene	10–30	3	MB	Kim et al. (2012)
TiO_2/graphene	5–40	1	2,4-dichlorophenoxyacetic acid and reactive red 195	Ghasemi et al. (2013)
TiO_2/graphene	–	1–10	MO	Khalid et al. (2013a)
TiO_2/graphene	10–15	10.8	RhB	Lei et al. (2012)
TiO_2/graphene	5 nm pore diameter	1	RhB and norfloxacin	Li et al. (2012)
TiO_2/graphene	20–200	–	MB	Pan et al. (2012)
TiO_2/graphene	12.3–41.0	–	Butane	Štengl et al. (2011)
TiO_2/graphene	18	–	RhB	Wang et al. (2011b)
ZnO/Ag/graphene	∼200		RhB	Xu et al. (2013a)
CdSe/graphene/TiO_2	–	34.22	MO and RhB	Ghosh et al. (2013a)
ZnO/graphene	20	–	MB and MO	Ahmad et al. (2013b)
ZnO/graphene	6	–	MB	Fu et al. (2013)
Graphene/ZnO	∼10	–	RhB	Saravanakumar et al. (2013)
Graphene/Ag-ZnO	32	10	MB, RhB and MO	Ahmad et al. (2013a)
CdSe/graphene	∼10	54.08	MO and RhB	Ghosh et al. (2013b)
PbS-graphene/TiO_2	∼15–19 for TiO_2 ∼20–25 for PbS	–	MB	Ullah et al. (2014)
$ZnFe_2O_4$/graphene	5	–	RhB, MO and MB	Lu et al. (2013)

(continued)

Table 1.2 (continued)

Graphene composites	Particle size (nm)	Graphene contents (wt.%)	Pollutants	References
Graphene/$InNbO_4$	5	–	MB and 2,4-dichlorophenol	Zhang et al. (2011b)
Graphene/γ-Bi_2MoO_6	10	1.0	MB	Zhou et al. (2011)
Graphene/Bi_2MoO_6	–	–	Reactive brilliant red dye	Wang et al. (2012b)
Graphene/$La_2Ti_2O_7$	400	–	RhB	Wu et al. (2011a)
$BiVO_4$/graphene	88	–	MB	Gawande and Thakare (2012)
Ag_3PO_4/graphene	250	–	RhB, MO, and MB	Yang et al. (2013b)
Graphene/BiOBr	–	~1.0	Sulforhodamine 640 dye	Zhang et al. (2012b)

1.8 Principles of Graphene/Semiconductor Composites

The low efficient "trial-and-error" approach immensely increased the workload of some experimental research. However, there has been extreme demand for theoretical guided design of better photocatalyst materials to ease the burden of experimental "trial-and-error" approach. The ability of photocatalytic materials in charge generation and light absorption relies greatly on its electronic band structures. Complementary to these effects, theoretical simulations have been indispensable in evaluating structural stabilities, electronic properties, work functions, charge transfer, and carrier effective mass of several semiconductor photocatalyst materials. In analyzing the charge generation ability of photocatalysts, first-principle simulations using quantum mechanics, such as density functional theory (DFT) and ab initio calculations, are able to explore the optical and electronic properties of semiconductor photocatalysts without experimental parameters. Generally, theoretical calculations can offer a perfect understanding for designing photocatalysts from the perspective of mechanisms. The ab initio prediction of semiconductors requires a precise theoretical explanation of many-body systems, and this has been the biggest problem in solid-state sciences (Li et al. 2017). The electronic Schrödinger equation can be explicitly solved using the Hartree–Fock method by expanding the wave function in the Slater determinant (Szabo and Ostlund 2012). However, this method normally neglects the electron correlation with the underestimation of the bond energies. The electron correlation corrections have been included using the post Hartree–Fock method with expanded determinants, but it is only limited to simple

systems (Szabo and Ostlund 2012). Moreover, the complicated N-electron wave function has proved to be unnecessary, and the total electron density can check the ground-state properties (Hohenberg and Kohn 1964; Kohn and Sham 1965). The DFT method proposed by Hohenberg, Kohn, and Sham decreases the complexity of the many-body Schrödinger equation into a series of Kohn–Sham single particle (Li et al. 2017). In the Kohn–Sham Hamiltonian, everything is known, apart from the exchange–correlation functional (Li et al. 2017). Therefore, the accuracy of DFT is due to its consideration of the exchange–correlation functional. Among the several types of the exchange–correlation functional that have been used in photocatalysis, the generalized gradient approximation (Perdew 1986) and the local density approximation (Kohn and Sham 1965) are the most common ones. The local density approximation works well for metallic systems but not for insulators and semiconductors, for which band gaps are underestimated (Li et al. 2017). The generalized gradient approximation (Becke 1988) is more accurate than the local density approximation since the generalized gradient approximation considers the inhomogeneity of electron density. Higher-order derivatives of electron density with the meta-generalized gradient approximation functionals can enhance the chemical accuracy of photocatalyst systems with severe variations of electron density (Li et al. 2017). Nonetheless, the delocalized effects of the generalized gradient approximation and meta-generalized gradient approximation are intrinsically localized (Li et al. 2017). The delocalized effects are treated by replacing the exchange–correlation energy with the exact Hartree–Fock exchange–correlation energy. The hybrid Heyd–Scuseria–Ernzerhof functional (Heyd et al. 2003) mixes the nonlocal Hartree–Fock exchange with the local/semi-local density functional theory exchange which enhances the accuracy of electronic structures (Muscat et al. 2001). Moreover, adding a Hubbard parameter (U) to the generalized gradient approximation and the local density approximation (DFT + U) calculation also improves the band structure depending on the choice of several empirical parameters (Anisimov et al. 1997). The DFT + U and hybrid Heyd–Scuseria–Ernzerhof functional have been more robust and reliable with progress in solid-state materials science, solid-state physics, chemistry, and chemical engineering (Lejaeghere et al. 2016). Hence, new photocatalyst materials with several structural characteristics, electronic structure (band structure, electron density distributions, the density of state, and charge population), and compositions are continuously studied using DFT calculations. For example, Geng et al. (2013b) carried out DFT calculations to understand the influence of interface structure on the photocatalytic property of ZnO/graphene composites. The authors established that the weak interactions between ZnO monolayer and graphene sheets have no influence on the electronic properties of graphene. Moreover, stronger binding energies and larger charge transfers were observed for thick ZnO slabs with polarized surfaces on the graphene sheet. Coupling graphene sheets on the surface of ZnO with O termination showed lower work function and p-type conductivity, while graphene sheets on the surface of ZnO with Zn termination exhibited higher work function and n-type conductivity. Through the conjugate gradient minimization method with the norm-conserving pseudopotential and the double-zeta plus polarization basis sets,

the synergistic effect of TiO_2/graphene/MoS_2 ternary nanocomposites was investigated (Yuan et al. 2015). It was discovered that the electron excites from TiO_2 cluster to graphene to reduce the band gap of the nanocomposites. Within the local density approximation scheme with the norm-conserving pseudopotential and the plane-wave basis set, the improved absorption of TiO_2(001)/graphene nanocomposites in the visible region was influenced by the graphene hybridization (Gao et al. 2013). The energy bands and the projected density of state results offer much information on the photocatalytic mechanism with electron migrations from O 2p state to the C 2p state of the nanocomposites. The improved charge migration and visible light absorption of graphene/Bi_2WO_6(010) (Ren et al. 2016), graphene/rutile TiO_2 (Du et al. 2011; Long 2013), graphene/anatase TiO_2 (Li et al. 2013b), and ZnO (Pengtao et al. 2013) nanocomposites were ascribed to the large interfacial work function difference. The interfacial interaction between graphene and ZnO (Pengtao et al. 2013), $SrTiO_3$ (Yang et al. 2015), and Ag_3PO_4 (Xu et al. 2014) nanocomposites was due to van der Waal interactions based on the DFT-D2 approach proposed by Grimme (2004, 2006). A higher stability was found in the Fe-doped TiO_2/graphene nanocomposite compared to the TiO_2/GR nanocomposite (Nasrin et al. 2014). This is due to the higher charge carrier transfer from Fe-doped TiO_2 to the GR sheets. The adsorption of TiO_2 on pristine graphene nanoribbons and functionalized graphene was also studied using the generalized gradient approximation functional of the Perdew–Wang 91 and projector augmented wave method (Ayissi et al. 2013). A large physical adsorption was found for the nanocomposites on all the chemical adsorption sites of the graphene sheets and functionalized graphene nanoribbons. Using the semi-core pseudopotential method and the hybrid HSE06 functional, the chemical and electronic structures of titania/graphene and titania/graphdiyne (GD) nanocomposites with different titania facets were explored (Yang et al. 2013a). Higher oxidation properties and charge separation of TiO_2(001)/GD composite compared with the TiO_2(001)/GR and TiO_2(001) composite were observed. Geng et al. (2013a) used DFT to investigate the enhanced photocatalytic performance of TiO_2/graphene composites. The TiO_2 clusters were coupled with monovacancy graphene (V-G), epoxy graphene (O-G), and pristine graphene (P-G). The stability of TiO_2 coupled with V-G and O-G was higher than the P-G based on the binding energy and geometric configurations results. The improved photoactivity of the nanocomposites was as a result of the reduced electrons and holes recombination rate, as well as the decrease excitation energy in the visible region.

1.9 Conclusion

During the past decades, much effort has been made to comprehend how graphene-based materials can be utilized to solve water remediation issues. The inherent properties of graphene, such as large surface area, excellent electron mobility, high mechanical strength, and large thermal conductivity, have opened new opportunities

to enhance the activity of several semiconductors. In this book chapter, several types of graphene/semiconductor composites have been discussed for environmental remediation application. We have selectively discussed the fundamentals, basic principles, and mechanism of semiconductor photocatalysts. In addition, the preparation, properties, characterization techniques, and applications of graphene-based materials in water purification have also been emphasized. The photocatalytic performance toward the removal of heavy metal ions and degradation of contaminants was synergistically improved when graphene was coupled with semiconductors. The size-dependent properties of semiconductors together with the unique properties of graphene induce further functionalities, such as the prolonged visible light absorption edge, enhanced charge separation properties, high adsorption capacity, and stability of the composites.

We have illustrated how theoretical studies have used to explain the photocatalytic behavior of semiconductor. Electronic structure calculations have shown how interface is significant to determine the photocatalytic activity and adsorption behavior of semiconductor photocatalyst materials. This book chapter mentions how first-principle studies can be applied routinely to study charge transfer and electronic properties of materials, which are often challenging to study experimentally.

Several fabrication methods have developed for both in situ and ex situ processing of semiconductor nanoparticles on the graphene sheet; however, some pressing issues must be addressed before large-scale application of these nanocomposites can be effectively achieved. Thus, the technology for fabricating high-quality graphene is still at the fundamental stage; further improvements are needed since the accurate control of the final product in terms of defect sites, reaggregation, purity, the number of layers, and control of defects is yet to be established. Moreover, large surface area architectures (graphene-based xerogels and aerogels) must be applied for heavy metal ions removal using the adsorption technique because the high surface area, nanoporosity, and microstructures of graphene show excellent adsorption capabilities of pollutants and heavy metal ions.

The design and fabrication of novel photocatalyst materials are one of the key research goals. The existing photocatalytic materials have several drawbacks, such as high cost, large band gaps, low active surface area, etc. It is of great significance to find cost-effective and advanced materials to prepare composite photocatalysts for practical applications. A perfect material for engineering composites should fulfill several requirements, such as visible light activity, high solar conversion efficiency, proper band-gap structure for redox reactions, high photostability for long-term applications, and scalability for commercialization.

Currently, the hybrid HSE06 functionals, which can precisely describe the electronic structures, cannot clearly offer a solution to the long-range van der Waals interaction in graphene-based composite materials. Thus, new functionals and codes, which can precisely address both the van der Waals interactions and electron correlation effects, are significant. This will become a key tool for hastening the design of advanced materials for water purification.

Acknowledgments The authors would like to acknowledge the financial contributions from the Faculty of Science: University of Johannesburg, South Africa, Department of Applied Chemistry and the National Research Foundation (TTK14052167682). FO acknowledges the financial support from the Global Excellence and Stature (GES) Doctoral Scholarship: University of Johannesburg, South Africa. EMK also acknowledges the financial support from National Research Foundation (NRF).

References

Ahmad M, Ahmed E, Hong ZL, Khalid NR, Ahmed W, Elhissi A (2013a) Graphene–Ag/ZnO nanocomposites as high performance photocatalysts under visible light irradiation. J Alloys Compd 577:717–727. https://doi.org/10.1016/j.jallcom.2013.06.137

Ahmad M, Ahmed E, Hong ZL, Xu JF, Khalid NR, Elhissi A, Ahmed W (2013b) A facile one-step approach to synthesizing ZnO/graphene composites for enhanced degradation of methylene blue under visible light. Appl Surf Sci 274:273–281. https://doi.org/10.1016/j.apsusc.2013.03.035

Ai L, Zhang C, Chen Z (2011) Removal of methylene blue from aqueous solution by a solvothermal-synthesized graphene/magnetite composite. J Hazard Mater 192:1515–1524. https://doi.org/10.1016/j.jhazmat.2011.06.068

Ali I, Gupta V (2006) Advances in water treatment by adsorption technology. Nat Protoc 1:2661–2667

Allen MJ, Tung VC, Kaner RB (2009) Honeycomb carbon: a review of graphene. Chem Rev 110:132–145

Alyüz B, Veli S (2009) Kinetics and equilibrium studies for the removal of nickel and zinc from aqueous solutions by ion exchange resins. J Hazard Mater 167:482–488

An X, Jimmy CY, Wang Y, Hu Y, Yu X, Zhang G (2012) WO_3 nanorods/graphene nanocomposites for high-efficiency visible-light-driven photocatalysis and NO_2 gas sensing. J Mater Chem 22:8525–8531

Anisimov VI, Aryasetiawan F, Lichtenstein A (1997) First-principles calculations of the electronic structure and spectra of strongly correlated systems: the LDA + U method. J Phys Condens Matter 9:767–808

Anpo M, Kamat P (2010) Environmental benign photocatalysts. In: Applications of titanium oxide-based materials. Springer, New York, pp 1–501

Ayissi S, Charpentier PA, Farhangi N, Wood JA, Palotás K, Hofer WA (2013) Interaction of titanium oxide nanostructures with graphene and functionalized graphene nanoribbons: a DFT study. J Phys Chem C 117:25424–25432. https://doi.org/10.1021/jp403835m

Bai X, Wang L, Zhu Y (2012) Visible photocatalytic activity enhancement of $ZnWO_4$ by graphene hybridization. ACS Catal 2:2769–2778

Bai S, Jiang J, Zhang Q, Xiong Y (2015) Steering charge kinetics in photocatalysis: intersection of materials syntheses, characterization techniques and theoretical simulations. Chem Soc Rev 44:2893–2939

Bard AJ, Parsons R, Jordan J (1985) Standard potentials in aqueous solution, vol 6. CRC press, New York, pp 1–829

Becke AD (1988) Density-functional exchange-energy approximation with correct asymptotic behavior. Phys Rev A 38:3098–3100

Berera R, van Grondelle R, Kennis JT (2009) Ultrafast transient absorption spectroscopy: principles and application to photosynthetic systems. Photosynth Res 101:105–118

Berger C, Song Z, Li X, Wu X, Brown N, Naud C, Mayou D, Li T, Hass J, Marchenkov AN (2006) Electronic confinement and coherence in patterned epitaxial graphene. Science 312:1191–1196

Bhatnagar A, Hogland W, Marques M, Sillanpää M (2013) An overview of the modification methods of activated carbon for its water treatment applications. Chem Eng J 219:499–511
Blake P, Hill E, Castro Neto A, Novoselov K, Jiang D, Yang R, Booth T, Geim A (2007) Making graphene visible. Appl Phys Lett 91:063124
Boehm H, Setton R, Stumpp E (1986) Nomenclature and terminology of graphite intercalation compounds. Carbon 24:241–245
Cai W, Yu J, Mann S (2009) Template-free hydrothermal fabrication of hierarchically organized γ-AlOOH hollow microspheres. Microporous Mesoporous Mater 122:42–47
Cao S, Low J, Yu J, Jaroniec M (2015) Polymeric photocatalysts based on graphitic carbon nitride. Adv Mater 27:2150–2176
Casbeer E, Sharma VK, Li X-Z (2012) Synthesis and photocatalytic activity of ferrites under visible light: a review. Sep Purif Technol 87:1–14
Chandra V, Park J, Chun Y, Lee JW, Hwang I-C, Kim KS (2010) Water-dispersible magnetite-reduced graphene oxide composites for arsenic removal. ACS Nano 4:3979–3986
Chandra S, Das P, Bag S, Bhar R, Pramanik P (2012) Mn_2O_3 decorated graphene nanosheet: an advanced material for the photocatalytic degradation of organic dyes. Mater Sci Eng B 177:855–861
Chang Y-C (2014) ZnO nanopinecone arrays with enhanced photocatalytic performance in sunlight. RSC Adv 4:20273–20280
Chang Y-P, Ren C-L, Qu J-C, Chen X-G (2012) Preparation and characterization of Fe_3O_4/graphene nanocomposite and investigation of its adsorption performance for aniline and p-chloroaniline. Appl Surf Sci 261:504–509. https://doi.org/10.1016/j.apsusc.2012.08.045
Chen T, Feng Z, Wu G, Shi J, Ma G, Ying P, Li C (2007) Mechanistic studies of photocatalytic reaction of methanol for hydrogen production on Pt/TiO_2 by in situ Fourier transform IR and time-resolved IR spectroscopy. J Phys Chem C 111:8005–8014
Chen C, Ma W, Zhao J (2010) Semiconductor-mediated photodegradation of pollutants under visible-light irradiation. Chem Soc Rev 39:4206–4219
Chong MN, Jin B, Chow CW, Saint C (2010) Recent developments in photocatalytic water treatment technology: a review. Water Res 44:2997–3027
Compton OC, Nguyen ST (2010) Graphene oxide, highly reduced graphene oxide, and graphene: versatile building blocks for carbon-based materials. Small 6:711–723
Dąbrowski A (2001) Adsorption—from theory to practice. Adv Colloid Interf Sci 93:135–224
Du A, Ng YH, Bell NJ, Zhu Z, Amal R, Smith SC (2011) Hybrid graphene/titania nanocomposite: Interface charge transfer, hole doping, and sensitization for visible light response. J Phys Chem Lett 2:894–899. https://doi.org/10.1021/jz2002698
Emtsev KV, Bostwick A, Horn K, Jobst J, Kellogg GL, Ley L, McChesney JL, Ohta T, Reshanov SA, Röhrl J (2009) Towards wafer-size graphene layers by atmospheric pressure graphitization of silicon carbide. Nat Mater 8:203–207
Fageria P, Gangopadhyay S, Pande S (2014) Synthesis of ZnO/Au and ZnO/Ag nanoparticles and their photocatalytic application using UV and visible light. RSC Adv 4:24962–24972
Fan H, Zhao X, Yang J, Shan X, Yang L, Zhang Y, Li X, Gao M (2012) ZnO–graphene composite for photocatalytic degradation of methylene blue dye. Catal Commun 29:29–34
Farhangi N, Chowdhury RR, Medina-Gonzalez Y, Ray MB, Charpentier PA (2011) Visible light active Fe doped TiO_2 nanowires grown on graphene using supercritical CO_2. Appl Catal B 110:25–32
Ferrari AC, Meyer J, Scardaci V, Casiraghi C, Lazzeri M, Mauri F, Piscanec S, Jiang D, Novoselov K, Roth S (2006) Raman spectrum of graphene and graphene layers. Phys Rev Lett 97:187401
Feynman RP, Leighton RB, Sands M (2013) The Feynman lectures on physics, desktop edition volume I, vol 1. Basic books, New York, pp 1–52
Friedmann D, Mendive C, Bahnemann D (2010) TiO_2 for water treatment: parameters affecting the kinetics and mechanisms of photocatalysis. Appl Catal B 99:398–406

Friedmann D, Hakki A, Kim H, Choi W, Bahnemann D (2016) Heterogeneous photocatalytic organic synthesis: state-of-the-art and future perspectives. Green Chem 18:5391–5411

Fu F, Wang Q (2011a) Removal of heavy metal ions from wastewaters: a review. J Environ Manag 92:407–418

Fu Y, Wang X (2011b) Magnetically separable $ZnFe_2O_4$–graphene catalyst and its high photocatalytic performance under visible light irradiation. Ind Eng Chem Res 50:7210–7218

Fu Y, Sun X, Wang X (2011) $BiVO_4$–graphene catalyst and its high photocatalytic performance under visible light irradiation. Mater Chem Phys 131:325–330. https://doi.org/10.1016/j.matchemphys.2011.09.049

Fu Y, Chen H, Sun X, Wang X (2012) Combination of cobalt ferrite and graphene: high-performance and recyclable visible-light photocatalysis. Appl Catal B 111:280–287

Fu D, Han G, Yang F, Zhang T, Chang Y, Liu F (2013) Seed-mediated synthesis and the photodegradation activity of ZnO–graphene hybrids excluding the influence of dye adsorption. Appl Surf Sci 283:654–659. https://doi.org/10.1016/j.apsusc.2013.07.003

Fujishima A, Honda K (1972) Electrochemical photolysis of water at a semiconductor electrode. Nature 238:37–38

Ganzenko O, Huguenot D, Van Hullebusch ED, Esposito G, Oturan MA (2014) Electrochemical advanced oxidation and biological processes for wastewater treatment: a review of the combined approaches. Environ Sci Pollut Res 21:8493–8524

Gao E, Wang W, Shang M, Xu J (2011) Synthesis and enhanced photocatalytic performance of graphene-Bi_2WO_6 composite. Phys Chem Chem Phys 13:2887–2893

Gao Z, Liu J, Xu F, Wu D, Wu Z, Jiang K (2012a) One-pot synthesis of graphene–cuprous oxide composite with enhanced photocatalytic activity. Solid State Sci 14:276–280

Gao Z, Liu N, Wu D, Tao W, Xu F, Jiang K (2012b) Graphene–CdS composite, synthesis and enhanced photocatalytic activity. Appl Surf Sci 258:2473–2478. https://doi.org/10.1016/j.apsusc.2011.10.075

Gao H, Li X, Lv J, Liu G (2013) Interfacial charge transfer and enhanced photocatalytic mechanisms for the hybrid graphene/Anatase TiO_2(001) nanocomposites. J Phys Chem C 117:16022–16027. https://doi.org/10.1021/jp403241d

Gao C, Wang J, Xu H, Xiong Y (2017) Coordination chemistry in the design of heterogeneous photocatalysts. Chem Soc Rev 46:2799–2823

Gawande SB, Thakare SR (2012) Graphene wrapped $BiVO_4$ photocatalyst and its enhanced performance under visible light irradiation. Int Nano Lett 2:1–7. https://doi.org/10.1186/2228-5326-2-11

Gawande SB, Thakare SR (2013) Synthesis of visible light active graphene-modified $BaCrO_4$ nanocomposite photocatalyst. Int Nano Lett 3:1–8

Geim AK (2009) Graphene: status and prospects. Science 324:1530–1534

Geng W, Liu H, Yao X (2013a) Enhanced photocatalytic properties of titania–graphene nanocomposites: a density functional theory study. Phys Chem Chem Phys 15:6025–6033

Geng W, Zhao X, Liu H, Yao X (2013b) Influence of interface structure on the properties of ZnO/graphene composites: a theoretical study by density functional theory calculations. J Phys Chem C 117:10536–10544

Ghasemi S, Setayesh SR, Habibi-Yangjeh A, Hormozi-Nezhad MR, Gholami MR (2012) Assembly of CeO_2–TiO_2 nanoparticles prepared in room temperature ionic liquid on graphene nanosheets for photocatalytic degradation of pollutants. J Hazard Mater 199:170–178. https://doi.org/10.1016/j.jhazmat.2011.10.080

Ghasemi S, Esfandiar A, Rahman Setayesh S, Habibi-Yangjeh A, Iraji zad A, Gholami MR (2013) Synthesis and characterization of TiO_2–graphene nanocomposites modified with noble metals as a photocatalyst for degradation of pollutants. Appl Catal A 462:82–90. https://doi.org/10.1016/j.apcata.2013.04.029

Ghosh T, Cho K-Y, Ullah K, Nikam V, Park C-Y, Meng Z-D, Oh W-C (2013a) High photonic effect of organic dye degradation by CdSe–graphene–TiO_2 particles. J Ind Eng Chem 19:797–805. https://doi.org/10.1016/j.jiec.2012.10.020

Ghosh T, Ullah K, Nikam V, Park C-Y, Meng Z-D, Oh W-C (2013b) The characteristic study and sonocatalytic performance of CdSe–graphene as catalyst in the degradation of azo dyes in aqueous solution under dark conditions. Ultrason Sonochem 20:768–776. https://doi.org/10.1016/j.ultsonch.2012.09.005

Grimme S (2004) Accurate description of van der Waals complexes by density functional theory including empirical corrections. J Comput Chem 25:1463–1473

Grimme S (2006) Semiempirical GGA-type density functional constructed with a long-range dispersion correction. J Comput Chem 27:1787–1799

Gu L, Wang J, Zou Z, Han X (2014) Graphitic-C_3N_4-hybridized TiO_2 nanosheets with reactive {001} facets to enhance the UV- and visible-light photocatalytic activity. J Hazard Mater 268:216–223

Guo S, Dong S (2011) Graphene nanosheet: synthesis, molecular engineering, thin film, hybrids, and energy and analytical applications. Chem Soc Rev 40:2644–2672

Guo H-L, Wang X-F, Qian Q-Y, Wang F-B, Xia X-H (2009) A green approach to the synthesis of graphene nanosheets. ACS Nano 3:2653–2659

Guo J, Zhu S, Chen Z, Li Y, Yu Z, Liu Q, Li J, Feng C, Zhang D (2011) Sonochemical synthesis of TiO_2 nanoparticles on graphene for use as photocatalyst. Ultrason Sonochem 18:1082–1090

Guo J, Wang R, Tjiu WW, Pan J, Liu T (2012) Synthesis of Fe nanoparticles@graphene composites for environmental applications. J Hazard Mater 225:63–73. https://doi.org/10.1016/j.jhazmat.2012.04.065

Gupta VK, Ali I, Saleh TA, Nayak A, Agarwal S (2012) Chemical treatment technologies for waste-water recycling-an overview. RSC Adv 2:6380–6388

Hao L, Song H, Zhang L, Wan X, Tang Y, Lv Y (2012) SiO_2/graphene composite for highly selective adsorption of Pb (II) ion. J Colloid Interface Sci 369:381–387. https://doi.org/10.1016/j.jcis.2011.12.023

He F, Fan J, Ma D, Zhang L, Leung C, Chan HL (2010) The attachment of Fe_3O_4 nanoparticles to graphene oxide by covalent bonding. Carbon 48:3139–3144

Hernandez Y, Nicolosi V, Lotya M, Blighe FM, Sun Z, De S, McGovern IT, Holland B, Byrne M, Gun'Ko YK, Boland JJ, Niraj P, Duesberg G, Krishnamurthy S, Goodhue R, Hutchison J, Scardaci V, Ferrari AC, Coleman JN (2008) High-yield production of graphene by liquid-phase exfoliation of graphite. Nat Nanotechnol 3:563–568. http://www.nature.com/nnano/journal/v3/n9/suppinfo/nnano.2008.215_S1.html

Heyd J, Scuseria GE, Ernzerhof M (2003) Hybrid functionals based on a screened Coulomb potential. J Chem Phys 118:8207–8215

Hitoki G, Ishikawa A, Takata T, Kondo JN, Hara M, Domen K (2002) Ta_3N_5 as a novel visible light-driven photocatalyst ($\lambda < 600$ nm). Chem Lett 31:736–737

Hoffmann MR, Martin ST, Choi W, Bahnemann DW (1995) Environmental applications of semiconductor photocatalysis. Chem Rev 95:69–96

Hohenberg P, Kohn W (1964) Inhomogeneous electron gas. Phys Rev 136:B864–B671

Hontoria-Lucas C, López-Peinado A, López-González JD, Rojas-Cervantes M, Martin-Aranda R (1995) Study of oxygen-containing groups in a series of graphite oxides: physical and chemical characterization. Carbon 33:1585–1592

Hou H, Zhou R, Wu P, Wu L (2012) Removal of Congo red dye from aqueous solution with hydroxyapatite/chitosan composite. Chem Eng J 211:336–342

Hummers WS, Offeman RE (1958) Preparation of graphitic oxide. J Am Chem Soc 80:1339–1339. https://doi.org/10.1021/ja01539a017

Ismail AA, Geioushy R, Bouzid H, Al-Sayari SA, Al-Hajry A, Bahnemann DW (2013) TiO_2 decoration of graphene layers for highly efficient photocatalyst: impact of calcination at different gas atmosphere on photocatalytic efficiency. Appl Catal B 129:62–70

Jiao L, Wang X, Diankov G, Wang H, Dai H (2010) Facile synthesis of high-quality graphene nanoribbons. Nat Nanotechnol 5:321–325

Kapilashrami M, Zhang Y, Liu Y-S, Hagfeldt A, Guo J (2014) Probing the optical property and electronic structure of TiO_2 nanomaterials for renewable energy applications. Chem Rev 114:9662–9707

Katsnelson MI (2007) Graphene: carbon in two dimensions. Mater Today 10:20–27

Khalid N, Hong Z, Ahmed E, Zhang Y, Chan H, Ahmad M (2012a) Synergistic effects of Fe and graphene on photocatalytic activity enhancement of TiO_2 under visible light. Appl Surf Sci 258:5827–5834

Khalid NR, Ahmed E, Hong Z, Ahmad M (2012b) Synthesis and photocatalytic properties of visible light responsive La/TiO_2-graphene composites. Appl Surf Sci 263:254–259. https://doi.org/10.1016/j.apsusc.2012.09.039

Khalid N, Ahmed E, Hong Z, Sana L, Ahmed M (2013a) Enhanced photocatalytic activity of graphene–TiO_2 composite under visible light irradiation. Curr Appl Phys 13:659–663. https://doi.org/10.1016/j.cap.2012.11.003

Khalid N, Ahmed E, Hong Z, Zhang Y, Ullah M, Ahmed M (2013b) Graphene modified Nd/TiO_2 photocatalyst for methyl orange degradation under visible light irradiation. Ceram Int 39:3569–3575

Kim CH, Kim B-H, Yang KS (2012) TiO_2 nanoparticles loaded on graphene/carbon composite nanofibers by electrospinning for increased photocatalysis. Carbon 50:2472–2481

Kohn W, Sham LJ (1965) Self-consistent equations including exchange and correlation effects. Phys Rev 140:A1133–A1138

Kuzmenko A, Van Heumen E, Carbone F, Van Der Marel D (2008) Universal optical conductance of graphite. Phys Rev Lett 100:117401

Lee Y-C, Yang J-W (2012) Self-assembled flower-like TiO_2 on exfoliated graphite oxide for heavy metal removal. J Ind Eng Chem 18:1178–1185

Lei Z, Ghosh T, Chong-Yeon P, Ze-Da M, Won-Chun O (2012) Enhanced sonocatalytic degradation of rhodamine B by graphene-TiO_2 composites synthesized by an ultrasonic-assisted method. Chin J Catal 33:1276–1283

Lejaeghere K, Bihlmayer G, Björkman T, Blaha P, Blügel S, Blum V, Caliste D, Castelli IE, Clark SJ, Dal Corso A, de Gironcoli S, Deutsch T, Dewhurst JK, Di Marco I, Draxl C, Dułak M, Eriksson O, Flores-Livas JA, Garrity KF, Genovese L, Giannozzi P, Giantomassi M, Goedecker S, Gonze X, Grånäs O, Gross EKU, Gulans A, Gygi F, Hamann DR, Hasnip PJ, Holzwarth NAW, Iuşan D, Jochym DB, Jollet F, Jones D, Kresse G, Koepernik K, Küçükbenli E, Kvashnin YO, Locht ILM, Lubeck S, Marsman M, Marzari N, Nitzsche U, Nordström L, Ozaki T, Paulatto L, Pickard CJ, Poelmans W, Probert MIJ, Refson K, Richter M, Rignanese G-M, Saha S, Scheffler M, Schlipf M, Schwarz K, Sharma S, Tavazza F, Thunström P, Tkatchenko A, Torrent M, Vanderbilt D, van Setten MJ, Van Speybroeck V, Wills JM, Yates JR, Zhang G-X, Cottenier S (2016) Reproducibility in density functional theory calculations of solids. Science 351:1–7

Li B, Cao H (2011) ZnO@graphene composite with enhanced performance for the removal of dye from water. J Mater Chem 21:3346–3349

Li D, Müller MB, Gilje S, Kaner RB, Wallace GG (2008) Processable aqueous dispersions of graphene nanosheets. Nat Nanotechnol 3:101–105

Li N, Zheng M, Chang X, Ji G, Lu H, Xue L, Pan L, Cao J (2011a) Preparation of magnetic $CoFe_2O_4$-functionalized graphene sheets via a facile hydrothermal method and their adsorption properties. J Solid State Chem 184:953–958. https://doi.org/10.1016/j.jssc.2011.01.014

Li Y, Zhang P, Du Q, Peng X, Liu T, Wang Z, Xia Y, Zhang W, Wang K, Zhu H (2011b) Adsorption of fluoride from aqueous solution by graphene. J Colloid Interface Sci 363:348–354

Li K, Chen T, Yan L, Dai Y, Huang Z, Guo H, Jiang L, Gao X, Xiong J, Song D (2012) Synthesis of mesoporous graphene and tourmaline co-doped titania composites and their photocatalytic activity towards organic pollutant degradation and eutrophic water treatment. Catal Commun 28:196–201

Li K, Chen T, Yan L, Dai Y, Huang Z, Xiong J, Song D, Lv Y, Zeng Z (2013a) Design of graphene and silica co-doped titania composites with ordered mesostructure and their simulated sunlight photocatalytic performance towards atrazine degradation. Colloids Surf A Physicochem Eng Asp 422:90–99

Li X, Gao H, Liu G (2013b) A LDA + U study of the hybrid graphene/anatase TiO_2 nanocomposites: interfacial properties and visible light response. Comput Theor Chem 1025:30–34. https://doi.org/10.1016/j.comptc.2013.10.006

Li X, Yu J, Low J, Fang Y, Xiao J, Chen X (2015) Engineering heterogeneous semiconductors for solar water splitting. J Mater Chem A 3:2485–2534
Li X, Yu J, Jaroniec M (2016) Hierarchical photocatalysts. Chem Soc Rev 45:2603–2636
Li Y, Li Y-L, Sa B, Ahuja R (2017) Review of two-dimensional materials for photocatalytic water splitting from a theoretical perspective. Catal Sci Technol 7:545–559. https://doi.org/10.1039/C6CY02178F
Liu J, Bai H, Wang Y, Liu Z, Zhang X, Sun DD (2010) Self-assembling TiO_2 Nanorods on large graphene oxide sheets at a two-phase Interface and their anti-recombination in photocatalytic applications. Adv Funct Mater 20:4175–4181
Liu S, Sun H, Liu S, Wang S (2013a) Graphene facilitated visible light photodegradation of methylene blue over titanium dioxide photocatalysts. Chem Eng J 214:298–303
Liu Y, Goebl J, Yin Y (2013b) Templated synthesis of nanostructured materials. Chem Soc Rev 42:2610–2653
Long R (2013) Understanding the electronic structures of graphene quantum dot Physisorption and chemisorption onto the TiO_2 (110) surface: a first-principles calculation. ChemPhysChem 14:579–582
Lou XW, Wang Y, Yuan C, Lee JY, Archer LA (2006) Template-free synthesis of SnO_2 hollow nanostructures with high lithium storage capacity. Adv Mater 18:2325–2329
Lü K, Zhao G, Wang X (2012) A brief review of graphene-based material synthesis and its application in environmental pollution management. Chin Sci Bull 57:1223–1234
Lu D, Zhang Y, Lin S, Wang L, Wang C (2013) Synthesis of magnetic $ZnFe_2O_4$/graphene composite and its application in photocatalytic degradation of dyes. J Alloys Compd 579:336–342. https://doi.org/10.1016/j.jallcom.2013.06.098
Lü W, Wu Y, Chen J, Yang Y (2014) Facile preparation of graphene–Fe_3O_4 nanocomposites for extraction of dye from aqueous solution. CrystEngComm 16:609–615
Lubchenco J (1998) Entering the century of the environment: a new social contract for science. Science 279:491–497
Luo Y-B, Shi Z-G, Gao Q, Feng Y-Q (2011) Magnetic retrieval of graphene: extraction of sulfonamide antibiotics from environmental water samples. J Chromatogr A 1218:1353–1358
Machado BF, Serp P (2012) Graphene-based materials for catalysis. Catal Sci Technol 2:54–75
Marahel F, Khan MA, Marahel E, Bayesti I, Hosseini S (2015) Kinetics, thermodynamics, and isotherm studies for the adsorption of BR2 dye onto avocado integument. Desalin Water Treat 53:826–835
McAllister MJ, Li J-L, Adamson DH, Schniepp HC, Abdala AA, Liu J, Herrera-Alonso M, Milius DL, Car R, Prud'homme RK (2007) Single sheet functionalized graphene by oxidation and thermal expansion of graphite. Chem Mater 19:4396–4404
Meng Z-D, Zhu L, Ghosh T, Park C-Y, Ullah K, Nikam V, Oh W-C (2012) Ag_2Se-graphene/TiO_2 nanocomposites, sonochemical synthesis and enhanced photocatalytic properties under visible light. Bull Kor Chem Soc 33:3761–3766
Min Y, Zhang K, Chen L, Chen Y, Zhang Y (2012) Ionic liquid assisting synthesis of ZnO/graphene heterostructure photocatalysts with tunable photoresponse properties. Diam Relat Mater 26:32–38
Min Y, He G, Li R, Zhao W, Chen Y, Zhang Y (2013) Doping nitrogen anion enhanced photocatalytic activity on TiO_2 hybridized with graphene composite under solar light. Sep Purif Technol 106:97–104
Mohanty K, Das D, Biswas MN (2008) Treatment of phenolic wastewater in a novel multi-stage external loop airlift reactor using activated carbon. Sep Purif Technol 58:311–319
Mori K, Yamashita H (2010) Progress in design and architecture of metal nanoparticles for catalytic applications. Phys Chem Chem Phys 12:14420–14432
Muscat J, Wander A, Harrison N (2001) On the prediction of band gaps from hybrid functional theory. Chem Phys Lett 342:397–401
Nasrin F, Serge A, Paul AC (2014) Fe doped TiO_2–graphene nanostructures: synthesis, DFT modeling and photocatalysis. Nanotechnology 25:1–11

Neppolian B, Bruno A, Bianchi CL, Ashokkumar M (2012) Graphene oxide based Pt–TiO_2 photocatalyst: ultrasound assisted synthesis, characterization and catalytic efficiency. Ultrason Sonochem 19:9–15

Novoselov KS, Geim AK, Morozov SV, Jiang D, Zhang Y, Dubonos SV, Grigorieva IV, Firsov AA (2004) Electric field effect in atomically thin carbon films. Science 306:666–669

Osgood R (2006) Photoreaction dynamics of molecular adsorbates on semiconductor and oxide surfaces. Chem Rev 106:4379–4401

Pan X, Zhao Y, Liu S, Korzeniewski CL, Wang S, Fan Z (2012) Comparing graphene-TiO_2 nanowire and graphene-TiO_2 nanoparticle composite photocatalysts. ACS Appl Mater Interfaces 4:3944–3950

Park S, An J, Jung I, Piner RD, An SJ, Li X, Velamakanni A, Ruoff RS (2009) Colloidal suspensions of highly reduced graphene oxide in a wide variety of organic solvents. Nano Lett 9:1593–1597

Pasternak S, Paz Y (2013) On the similarity and dissimilarity between photocatalytic water splitting and photocatalytic degradation of pollutants. ChemPhysChem 14:2059–2070

Pengtao X, Qing T, Zhen Z (2013) Structural and electronic properties of graphene–ZnO interfaces: dispersion-corrected density functional theory investigations. Nanotechnology 24:1–7

Perdew JP (1986) Density-functional approximation for the correlation energy of the inhomogeneous electron gas. Phys Rev B 33:8822–8824

Qi L, Cheng B, Yu J, Ho W (2016) High-surface area mesoporous Pt/TiO_2 hollow chains for efficient formaldehyde decomposition at ambient temperature. J Hazard Mater 301:522–530

Qu Y, Duan X (2013) Progress, challenge and perspective of heterogeneous photocatalysts. Chem Soc Rev 42:2568–2580

Qu J, Fan M (2010) The current state of water quality and technology development for water pollution control in China. Crit Rev Environ Sci Technol 40:519–560

Qu X, Alvarez PJ, Li Q (2013) Applications of nanotechnology in water and wastewater treatment. Water Res 47:3931–3946

Rahman MA (2015) A review on semiconductors including applications and temperature effects in semiconductors. Am Sci Res J Eng Technol Sci 7:50–70

Ramesha G, Kumara AV, Muralidhara H, Sampath S (2011) Graphene and graphene oxide as effective adsorbents toward anionic and cationic dyes. J Colloid Interface Sci 361:270–277

Rao C, Biswas K, Subrahmanyam K, Govindaraj A (2009) Graphene, the new nanocarbon. J Mater Chem 19:2457–2469

Ray S, Takafuji M, Ihara H (2013) Peptide-based surface modified silica particles: adsorption materials for dye-loaded wastewater treatment. RSC Adv 3:23664–23672

Ren Y, Yan N, Wen Q, Fan Z, Wei T, Zhang M, Ma J (2011) Graphene/δ-MnO_2 composite as adsorbent for the removal of nickel ions from wastewater. Chem Eng J 175:1–7

Ren Y, Yan N, Feng J, Ma J, Wen Q, Li N, Dong Q (2012) Adsorption mechanism of copper and lead ions onto graphene nanosheet/δ-MnO_2. Mater Chem Phys 136:538–544

Ren F, Zhang J, Wang Y, Yao W (2016) A graphene-coupled Bi_2WO_6 nanocomposite with enhanced photocatalytic performance: a first-principles study. Phys Chem Chem Phys 18:14113–14121. https://doi.org/10.1039/C6CP00458J

Saravanakumar B, Mohan R, Kim S-J (2013) Facile synthesis of graphene/ZnO nanocomposites by low temperature hydrothermal method. Mater Res Bull 48:878–883. https://doi.org/10.1016/j.materresbull.2012.11.048

Sato N (1998) Electrochemistry at metal and semiconductor electrodes. Elsevier, Amsterdam, pp 1–397

Schedin F, Geim A, Morozov S, Hill E, Blake P, Katsnelson M, Novoselov K (2007) Detection of individual gas molecules adsorbed on graphene. Nat Mater 6:652–655

Schneider J, Matsuoka M, Takeuchi M, Zhang J, Horiuchi Y, Anpo M, Bahnemann DW (2014) Understanding TiO_2 photocatalysis: mechanisms and materials. Chem Rev 114:9919–9986

Seema H, Kemp KC, Chandra V, Kim KS (2012) Graphene–SnO_2 composites for highly efficient photocatalytic degradation of methylene blue under sunlight. Nanotechnology 23:1–8

Singh V, Joung D, Zhai L, Das S, Khondaker SI, Seal S (2011) Graphene based materials: past, present and future. Prog Mater Sci 56:1178–1271

Some S, Kim Y, Hwang E, Yoo H, Lee H (2012) Binol salt as a completely removable graphene surfactant. Chem Commun 48:7732–7734

Štengl VC, Popelková D, Vláčil P (2011) TiO_2–graphene nanocomposite as high performance photocatalysts. J Phys Chem C 115:25209–25218

Subrahmanyam K, Panchakarla L, Govindaraj A, Rao C (2009) Simple method of preparing graphene flakes by an arc-discharge method. J Phys Chem C 113:4257–4259

Sun Y, Zhao Z, Dong F, Zhang W (2015) Mechanism of visible light photocatalytic NO_x oxidation with plasmonic Bi cocatalyst-enhanced $(BiO)_2CO_3$ hierarchical microspheres. Phys Chem Chem Phys 17:10383–10390

Szabo A, Ostlund NS (2012) Modern quantum chemistry: introduction to advanced electronic structure theory. McGraw-Hill, New York

Sze SM (2008) Semiconductor devices: physics and technology, 2nd edn. Wiley, New York

Tang Y, Luo S, Teng Y, Liu C, Xu X, Zhang X, Chen L (2012) Efficient removal of herbicide 2,4-dichlorophenoxyacetic acid from water using Ag/reduced graphene oxide co-decorated TiO_2 nanotube arrays. J Hazard Mater 241:323–330

Tao W, Chang J, Wu D, Gao Z, Duan X, Xu F, Jiang K (2013) Solvothermal synthesis of graphene-Sb_2S_3 composite and the degradation activity under visible light. Mater Res Bull 48:538–543. https://doi.org/10.1016/j.materresbull.2012.11.053

Tung VC, Allen MJ, Yang Y, Kaner RB (2009) High-throughput solution processing of large-scale graphene. Nat Nanotechnol 4:25–29

Ullah K, Meng Z-D, Ye S, Zhu L, Oh W-C (2014) Synthesis and characterization of novel PbS–graphene/TiO_2 composite with enhanced photocatalytic activity. J Ind Eng Chem 20:1035–1042. https://doi.org/10.1016/j.jiec.2013.06.040

Upadhyay RK, Soin N, Roy SS (2014) Role of graphene/metal oxide composites as photocatalysts, adsorbents and disinfectants in water treatment: a review. RSC Adv 4:3823–3851

USEPA (2014) Drinking water and groundwater quality standards. USEPA, New York

Van Bommel A, Crombeen J, Van Tooren A (1975) LEED and Auger electron observations of the SiC(0001) surface. Surf Sci 48:463–472

Vayssieres L (2010) On solar hydrogen and nanotechnology. Wiley, New York, pp 1–665

Wang Y, Shi R, Lin J, Zhu Y (2010) Significant photocatalytic enhancement in methylene blue degradation of TiO_2 photocatalysts via graphene-like carbon in situ hybridization. Appl Catal B 100:179–183

Wang C, Feng C, Gao Y, Ma X, Wu Q, Wang Z (2011a) Preparation of a graphene-based magnetic nanocomposite for the removal of an organic dye from aqueous solution. Chem Eng J 173:92–97

Wang Z, Mao F, Huang X, Huang Y, Feng S, Yi J, Zhang C, Wei H, Liu S (2011b) Orthogonal test design for preparation of TiO_2/Graphene composites and study on its photocatalytic activity. Rare Metals 30:271–275

Wang H, Zhang D, Yan T, Wen X, Shi L, Zhang J (2012a) Graphene prepared via a novel pyridine–thermal strategy for capacitive deionization. J Mater Chem 22:23745–23748

Wang P, Ao Y, Wang C, Hou J, Qian J (2012b) A one-pot method for the preparation of graphene–Bi_2MoO_6 hybrid photocatalysts that are responsive to visible-light and have excellent photocatalytic activity in the degradation of organic pollutants. Carbon 50:5256–5264

Wang W, Yu J, Xiang Q, Cheng B (2012c) Enhanced photocatalytic activity of hierarchical macro/mesoporous TiO_2–graphene composites for photodegradation of acetone in air. Appl Catal B 119:109–116

Wang H, Zhang D, Yan T, Wen X, Zhang J, Shi L, Zhong Q (2013a) Three-dimensional macroporous graphene architectures as high performance electrodes for capacitive deionization. J Mater Chem A 1:11778–11789

Wang W, Lu C, Ni Y, Xu Z (2013b) Fabrication of CNTs and GP/AuGP modified TiO_2 photocatalyst with two-channel electron conduction path for significantly enhanced photocatalytic activity. Appl Catal B 129:606–613

Wang W, Ma R, Wu Q, Wang C, Wang Z (2013c) Fabrication of magnetic microsphere-confined graphene for the preconcentration of some phthalate esters from environmental water and soybean milk samples followed by their determination by HPLC. Talanta 109:133–140

Wang W, Yu JC, Xia D, Wong PK, Li Y (2013d) Graphene and g-C_3N_4 nanosheets cowrapped elemental α-sulfur as a novel metal-free heterojunction photocatalyst for bacterial inactivation under visible-light. Environ Sci Technol 47:8724–8732

Wang Z, Du Y, Zhang F, Zheng Z, Zhang X, Feng Q, Wang C (2013e) Photocatalytic degradation of pendimethalin over Cu_2O/SnO_2/graphene and SnO_2/graphene nanocomposite photocatalysts under visible light irradiation. Mater Chem Phys 140:373–381

Wu C, Zhang Y, Li S, Zheng H, Wang H, Liu J, Li K, Yan H (2011a) Synthesis and photocatalytic properties of the graphene–$La_2Ti_2O_7$ nanocomposites. Chem Eng J 178:468–474. https://doi.org/10.1016/j.cej.2011.10.062

Wu Q, Zhao G, Feng C, Wang C, Wang Z (2011b) Preparation of a graphene-based magnetic nanocomposite for the extraction of carbamate pesticides from environmental water samples. J Chromatogr A 1218:7936–7942

Xiang Q, Yu J, Jaroniec M (2012) Graphene-based semiconductor photocatalysts. Chem Soc Rev 41:782–796

Xu T, Zhang L, Cheng H, Zhu Y (2011) Significantly enhanced photocatalytic performance of ZnO *via* graphene hybridization and the mechanism study. Appl Catal B 101:382–387

Xu F, Yuan Y, Wu D, Zhao M, Gao Z, Jiang K (2013a) Synthesis of ZnO/Ag/graphene composite and its enhanced photocatalytic efficiency. Mater Res Bull 48:2066–2070. https://doi.org/10.1016/j.materresbull.2013.02.034

Xu J, Lv H, Yang S-T, Luo J (2013b) Preparation of graphene adsorbents and their applications in water purification. Rev Inorg Chem 33:139–160

Xu L, Huang W-Q, Wang L-L, Huang G-F, Peng P (2014) Mechanism of superior visible-light photocatalytic activity and stability of hybrid Ag_3PO_4/graphene nanocomposite. J Phys Chem C 118:12972–12979

Yan Y, Sun S, Song Y, Yan X, Guan W, Liu X, Shi W (2013) Microwave-assisted in situ synthesis of reduced graphene oxide-$BiVO_4$ composite photocatalysts and their enhanced photocatalytic performance for the degradation of ciprofloxacin. J Hazard Mater 250:106–114

Yan X-G, Xu L, Huang W-Q, Huang G-F, Yang Z-M, Zhan S-Q, Long J-P (2014) Theoretical insight into the electronic and photocatalytic properties of Cu_2O from a hybrid density functional theory. Mater Sci Semicond Process 23:34–41

Yang L-Y, Dong S-Y, Sun J-H, Feng J-L, Wu Q-H, Sun S-P (2010) Microwave-assisted preparation, characterization and photocatalytic properties of a dumbbell-shaped ZnO photocatalyst. J Hazard Mater 179:438–443

Yang N, Liu Y, Wen H, Tang Z, Zhao H, Li Y, Wang D (2013a) Photocatalytic properties of Graphdiyne and graphene modified TiO_2: from theory to experiment. ACS Nano 7:1504–1512. https://doi.org/10.1021/nn305288z

Yang X, Cui H, Li Y, Qin J, Zhang R, Tang H (2013b) Fabrication of Ag_3PO_4-graphene composites with highly efficient and stable visible light photocatalytic performance. ACS Catal 3:363–369

Yang Y-C, Xu L, Huang W-Q, Luo C-Y, Huang G-F, Peng P (2015) Electronic structures and photocatalytic responses of $SrTiO_3$(100) surface interfaced with graphene, reduced graphene oxide, and Graphane: surface termination effect. J Phys Chem C 119:19095–19104. https://doi.org/10.1021/acs.jpcc.5b03630

Yao Y, Miao S, Liu S, Ma LP, Sun H, Wang S (2012) Synthesis, characterization, and adsorption properties of magnetic Fe_3O_4@graphene nanocomposite. Chem Eng J 184:326–332

Yoo D-H, Cuong TV, Pham VH, Chung JS, Khoa NT, Kim EJ, Hahn SH (2011) Enhanced photocatalytic activity of graphene oxide decorated on TiO_2 films under UV and visible irradiation. Curr Appl Phys 11:805–808

Yu JG, Guo H, Davis SA, Mann S (2006) Fabrication of hollow inorganic microspheres by chemically induced self-transformation. Adv Funct Mater 16:2035–2041

Yuan Q, Wu Z, Jin Y, Xu L, Xiong F, Ma Y, Huang W (2013) Photocatalytic cross-coupling of methanol and formaldehyde on a rutile TiO_2 (110) surface. J Am Chem Soc 135:5212–5219

Yuan Y, Gong X, Wang H (2015) The synergistic mechanism of graphene and MoS_2 for hydrogen generation: insights from density functional theory. Phys Chem Chem Phys 17:11375–11381. https://doi.org/10.1039/C5CP00011D

Yusoff N, Huang N, Muhamad M, Kumar S, Lim H, Harrison I (2013) Hydrothermal synthesis of CuO/functionalized graphene nanocomposites for dye degradation. Mater Lett 93:393–396. https://doi.org/10.1016/j.matlet.2012.10.015

Yusuf M, Elfghi F, Zaidi SA, Abdullah E, Khan MA (2015) Applications of graphene and its derivatives as an adsorbent for heavy metal and dye removal: a systematic and comprehensive overview. RSC Adv 5:50392–50420

Zhang K, Guo L (2013) Metal sulphide semiconductors for photocatalytic hydrogen production. Catal Sci Technol 3:1672–1690

Zhang H, Lv X, Li Y, Wang Y, Li J (2009) P25-graphene composite as a high performance photocatalyst. ACS Nano 4:380–386

Zhang N, Qiu H, Si Y, Wang W, Gao J (2011a) Fabrication of highly porous biodegradable monoliths strengthened by graphene oxide and their adsorption of metal ions. Carbon 49:827–837

Zhang X, Quan X, Chen S, Yu H (2011b) Constructing graphene/$InNbO_4$ composite with excellent adsorptivity and charge separation performance for enhanced visible-light-driven photocatalytic ability. Appl Catal B 105:237–242

Zhang Y, Tang Z-R, Fu X, Xu Y-J (2011c) Engineering the unique 2D mat of graphene to achieve graphene-TiO_2 nanocomposite for photocatalytic selective transformation: what advantage does graphene have over its forebear carbon nanotube? ACS Nano 5:7426–7435

Zhang D, Yan T, Shi L, Peng Z, Wen X, Zhang J (2012a) Enhanced capacitive deionization performance of graphene/carbon nanotube composites. J Mater Chem 22:14696–14704

Zhang X, Chang X, Gondal M, Zhang B, Liu Y, Ji G (2012b) Synthesis and photocatalytic activity of graphene/BiOBr composites under visible light. Appl Surf Sci 258:7826–7832

Zhang Z, Yang W, Zou X, Xu F, Wang X, Zhang B, Tang J (2012c) One-pot, solvothermal synthesis of TiO_2–graphene composite nanosheets. J Colloid Interface Sci 386:198–204

Zhao G, Song S, Wang C, Wu Q, Wang Z (2011) Determination of triazine herbicides in environmental water samples by high-performance liquid chromatography using graphene-coated magnetic nanoparticles as adsorbent. Anal Chim Acta 708:155–159

Zhou F, Shi R, Zhu Y (2011) Significant enhancement of the visible photocatalytic degradation performances of γ-Bi_2MoO_6 nanoplate by graphene hybridization. J Mol Catal A Chem 340:77–82. https://doi.org/10.1016/j.molcata.2011.03.012

Zhou M, Tian T, Li X, Sun X, Zhang J, Cui P, Tang J, Qin L-C (2014a) Production of graphene by liquid-phase exfoliation of intercalated graphite. Int J Electrochem Sci 9:810–820

Zhou P, Yu J, Jaroniec M (2014b) All-solid-state Z-scheme photocatalytic systems. Adv Mater 26:4920–4935

Zhu X, Zhang J, Chen F (2010) Hydrothermal synthesis of nanostructures $Bi_{12}TiO_{20}$ and their photocatalytic activity on acid orange 7 under visible light. Chemosphere 78:1350–1355

Zhu J, Wei S, Gu H, Rapole SB, Wang Q, Luo Z, Haldolaarachchige N, Young DP, Guo Z (2011) One-pot synthesis of magnetic graphene nanocomposites decorated with core@double-shell nanoparticles for fast chromium removal. Environ Sci Technol 46:977–985